GEOSCIENCE AUSTRALIA

Australian Government
Geoscience Australia

pmd*CRC

New Perspectives: The foundations and future of Australian exploration.

Abstracts for the June 2008 pmd*CRC Conference

R.J. Korsch & A.C. Barnicoat (editors)

Record
2008/09
Part 2

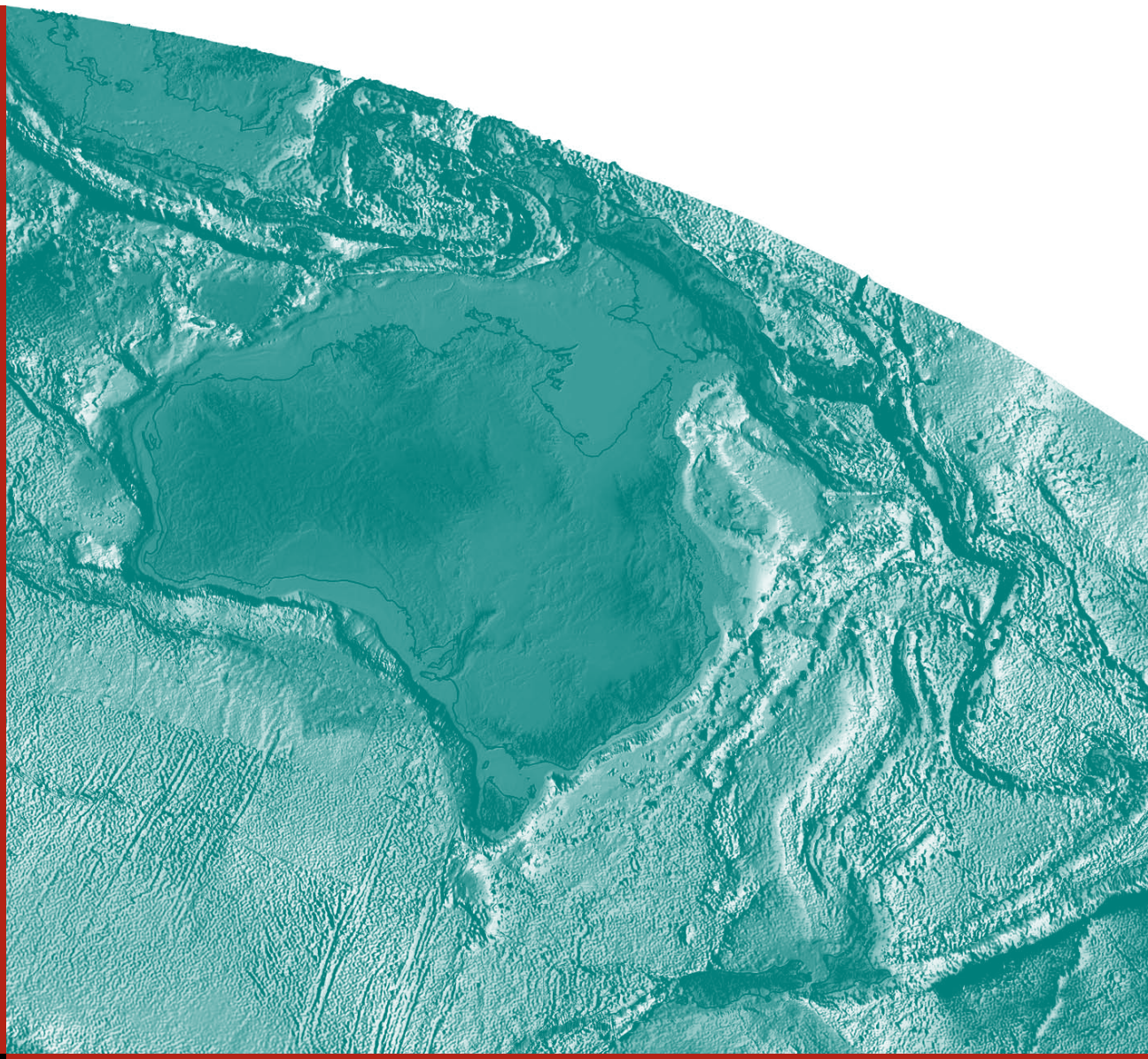

New perspectives: The foundations and future of Australian exploration

Abstracts for the June 2008 *pmd**CRC Conference

GEOSCIENCE AUSTRALIA

RECORD 2008/09

EDITED BY R. J. KORSCH AND A. C. BARNICOAT

*pmd**CRC, Geoscience Australia, GPO Box 378, Canberra, ACT 2601

Contents - part 2

Geodynamics: Modelling of large-scale processes

KLAUS REGENAUER-LIEB[1,2]

[1] School of Earth and Geographical Sciences, University of Western Australia, 35 Stirling Highway, Crawley, WA 6009
[2] CSIRO Exploration and Mining, Australian Resources Research Centre, 26 Dick Perry Avenue, Kensington WA 6151
Klaus.Regenauer-Lieb@csiro.au

Introduction

The physics and chemistry involved in the evolution of the surface of the "terrestrial planets", Mars, Earth and Venus, is thought to be controlled by their fundamentally different ways of heat transfer; these planets are largely composed of silicates and the study of their evolution is important because any self-consistent theory of planetary evolution should be capable of predicting the vastly different evolution of these three planets from the same set of fundamental principles. It turns out that these different paths of evolution arise from relatively small differences in initial conditions, largely dependent on the hydrogen content of the cores of these planets. Large scale geodynamics concerns itself with the evolution of the Earth using the evolution of the other two planets as constraints on the Earth's evolution. This evolution controls all the fundamental processes on Earth: the origin of the atmosphere and its subsequent evolution from essentially reduced (CO_2 rich) to oxidised (O_2-H_2O rich), the origin of the oceans and their chemical evolution, the development of plate tectonics (which did not occur on the other two planets), the progressive degassing of the Earth, and, ultimately, the origin of life about a quarter of the way through the present history of Earth.

Although there are clearly many important applications of this work, one of particular significance to Australia is the origin of giant ore bodies, since degassing/melting processes seem to be intimately linked to plate tectonics and, ultimately, to the setting of giant ore bodies. This research depends intimately on immediate access to state of the art high performance computing and on the maintenance of a network of the best minds in this field. The subject is innately multidisciplinary, arising from the vast range of spatial and temporal scales that need to be incorporated into the work. As such, nanoscale simulations of molecular structure and derived thermodynamic and transport parameters are just as important as modelling the interaction of mantle scale convection (the 3000 km between the lithosphere and the core of the Earth) with the chemical and mechanical evolution of the lithosphere (the top 100 km of the Earth). This research links in with a very active international research initiative on global planetary evolution modelling, with a glimpse into the unique Australian "time window" of the early evolution of the Earth.

This abstract summarises where geodynamic modelling techniques can presently assist the Australian mining industry for understanding large scale processes and where the future trends are.

Predictive Mineral Discovery and Geodynamic Modelling

We know that giant metal deposits are particularly associated with critical times in Earth history and locations in the Earth's crust. As an example, many gold deposits on Earth that we know today are

found to have been formed 2.6 billion years ago. Therefore, it is crucial to obtain an understanding of the global tectonics and an assessment of extreme events possibly affecting the whole of the Earth and their possible impact on these major episodes of metal release into the upper crust. Such events also have a long lasting effect on the making, shaping, preservation and locking in of the present life-sustaining plate tectonic regime. A critical point phenomenon exists where a small change in water content of the Earth's surface layer, the lithosphere, of only a few parts per million H/Si can have a fundamental effect on its mechanical strength (Regenauer-Lieb et al., 2001). Initial benchmark simulations on this critical point behaviour indicate that plate tectonics did not develop spontaneously but was probably accompanied by several major convective pulses (Muhlhaus & Regenauer-Lieb, 2005) associated with major fluid exchange to the surface. The potential to interpret global convection models in the light of episodicity and spatial patterning in metallogeny and geological data is a crucial challenge in economic geology. The focus is on looking into the more detailed processes that happen during the volatile flushing events.

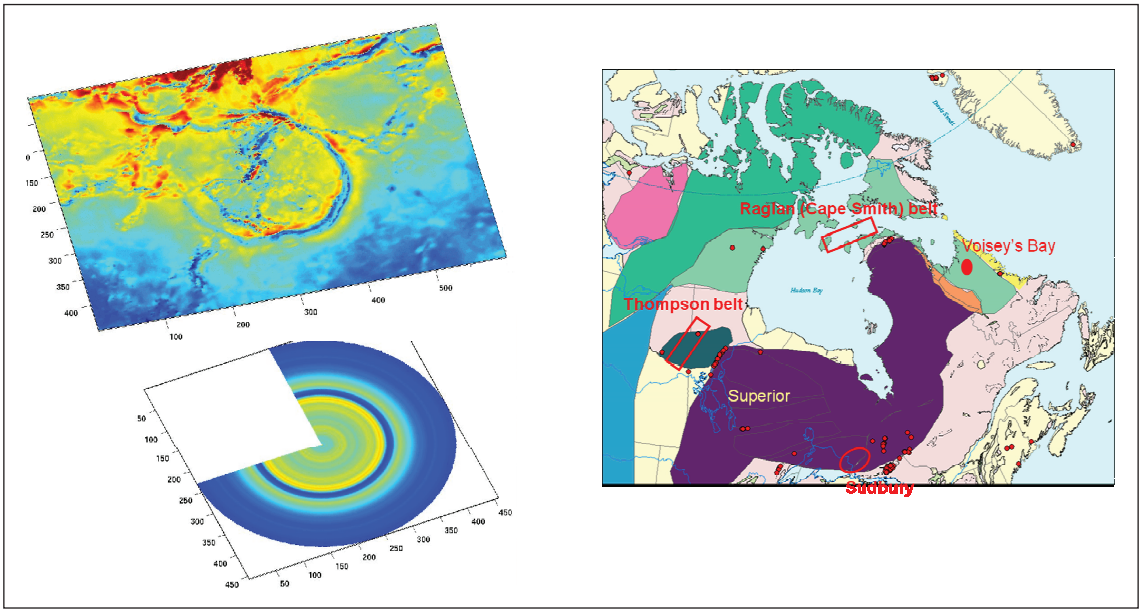

Figure 1: Some of the most unusual geological features on Venus are the so-called coronae. Coronae are very widespread on the Venusian surface; 360 are known. The largest and most prominent of all Coronae is Artemis Corona, a huge near circular structure with a diameter of approximately 2600 km (topography shown in top panel). The Corona shows a vertical relief of roughly six km from the surrounding chasms, to the highest point of its inner rim. The topography can be modeled by the impact of a very hot plume into the Venusian lithosphere (bottom panel). http://www.msi.umn.edu/~lilli/klaus-venus.pdf

Figure 2: On the present Earth, heat exchange through plumes is believed to be a minor component of the global heat budget. Heat is mainly exchanged through a steady mode of plate tectonics. Geodynamic modelling has, however, shown that plate tectonics is not likely to start immediately after the formation of the Earth. Episodic resurfacing events (dampened Venus style instabilities) are likely to have preceded the formation of plate tectonics in a transition period. These resurfacing events are triggered by giant subduction flushes and coupled giant plume events. One remnant of these events may be preserved in the nickel deposits surrounding the Superior Craton.

Conclusion and future work

Large scale geodynamic modelling is a powerful and robust tool that can be used to explore tectonic processes during the early history of the Earth. This method is presently underutilised in relation to predictive mineral discovery. The basic implication of basic modes of heat transfer in terrestrial planets

has been known in geodynamic modelling for quite some time (Moresi & Solomatov, 1998) and has been confirmed in numerous more sophisticated rheological setups, for example, Muhlhaus and Regenauer-Lieb (2005). The geodynamic modelling community has, so far, not delivered the message to the broader public of non-expert modellers. Geodynamic modelling can indeed be used as a hypothesis testing tool for mineral deposits on a large scale.

The next step of modelling is to extend the large-scale calculation down to the regional scale. It is still early days to judge whether this technique can directly be applied to predictive mineral discovery. Simplified thermodynamic approaches, however, already help to shed light on fundamental geological observations at local to regional scales. The first results are now available in recent manuscripts (Regenauer-Lieb et al., 2004, 2006; Rosenbaum et al., 2005; Hobbs et al., 2007; Weinberg et al., 2007). The results are encouraging in that crustal scale processes in geology, such as detachment faulting and metamorphic core complex formation and mid crustal folding, can be predicted self-consistently by simply extending a randomly perturbed homogenous piece of crust. The method is presently also extended to incorporate the modelling of volatile/melt transfer through the lithosphere.

Acknowledgements

This work grew out of the Computational Geosciences group in CSIRO Exploration and Mining and the ***pmd*CRC*** in collaboration with the Premiers Research Fellowship at the University of Western Australia. I would like to thank all collaborators, the Western Australian Government, the Minerals Down Under Flagship and the ***pmd*CRC*** for support.

References

Hobbs, B., Regenauer-Lieb, K. & Ord, A., 2007. The thermodynamics of folding in the middle to lower crust. Geology, 35(2), 175-178.

Moresi, L. & Solomatov, V., 1998. Mantle convection with a brittle lithosphere: thoughts on the global tectonic styles of the Earth and Venus. Geophysical Journal International, 133(3), 669-682.

Muhlhaus, H.B. & Regenauer-Lieb, K., 2005. Towards a self-consistent plate mantle model that includes elasticity: simple benchmarks and application to basic modes of convection. Geophysical Journal International, 163(2), 788-800.

Regenauer-Lieb, K., Hobbs, B. & Ord, A., 2004. On the thermodynamics of listric faults. Earth Planets Space, 56, 1111-1120.

Regenauer-Lieb, K., Weinberg, R.F. & Rosenbaum, G., 2006. The effect of energy feedbacks on continental strength. Nature, 442, 67-70.

Regenauer-Lieb, K., Yuen, D. & Branlund, J., 2001. The initation of subduction: criticality by addition of water? Science, 294, 578-580.

Rosenbaum, G., Regenauer-Lieb, K. & Weinberg, R.F., 2005. Continental extension: from core complexes to rigid block faulting. Geology, 33(7), 609-612.

Weinberg, R.F., Regenauer-Lieb, K. & Rosenbaum, G., 2007. Mantle detachment faults and the breakup of cold continental lithosphere. Geology, 35(11), 1035-1038.

A workflow for predictive discovery – thought processes, tools and target generation

PAUL A ROBERTS

*pmd**CRC*, CSIRO Exploration & Mining, Bentley, PO Box 1130, Bentley, WA 6102
Paul.a.roberts@csiro.au

Introduction

The *pmd**CRC* was established to assist Australian mineral explorers use an understanding of ore formation to improve targeting effectiveness, and thereby reduce ore discovery costs. One important focus of the CRC was to employ numerical modelling tools in the mineral exploration workflow. This abstract describes how the application of those tools can be integrated into the entire mineral exploration process, based principally on experience garnered during the life of the CRC.

Thought Processes

Important features of the thought processes in a process-driven targeting approach include:

- Abandon dependency on classic ore deposit classifications.
- Think globally, observe locally.
- Use all the data that you have before acquiring more.
- Observe for process and timing.

In the following section, these points are considered in some detail.

Abandon dependency on classic ore deposit classifications

Ore deposit classifications are a useful construct for teaching student geologists about ore formation and are also helpful for describing the types of geological associations that do exist in ore systems. However, if applied to mineral exploration, they can become a straitjacket for exploration model thinking. Empirical exploration practice commonly depends on using deposit-type descriptions as a template for developing prospect ranking schemes. This can prevent explorers from thinking about the significance of targeting criteria in terms of their actual importance in the formation of mineralisation within the area under investigation. For example, an exploration company might be seeking sediment-hosted base metal mineralisation in a new area. If it decides that the target is an 'MVT' as opposed to a 'sandstone-hosted lead deposit' or an 'Irish-type', this will drive ground selection and exploration strategies. Should the target turn out to look more like mineralisation on the Lennard Shelf or indeed a new variant in the continuum, there is a good chance that the explorer will look in the wrong place.

Think globally, observe locally

The process-driven approach recognises that a limited number of processes and parameters produce the bewildering array of observables that explorers see in real ore systems. The former are well described in

the 'Five Questions' descriptive framework (Price & Stoker, 2002; see also Barnicoat, this volume). At the district and the prospect scales, the explorer needs to be thinking about:

- Large scale structure controlling fluid and magma pathways.
- Permeability evolution and stress history before during and after mineralisation.
- Rheology contrasts preceding mineralisation and the pre-ore controls that may have produced those contrasts.
- The mineralogy of compartments within the Earth's crust and the consequences of them buffering fluids within them.
- The chemistry of fluids whether derived from rock-buffered compartments in the crust, meteoric water, the mantle or magmas.
- The influence of geological geometry and all of the foregoing factors on generating sustained physical or chemical gradients that will drive mineral precipitation over a long enough time to make an ore deposit.

These are the global controls on all hydrothermal ore systems. They manifest themselves in different ways in different terranes which is why slavish attention to standard ore deposit classifications is so risky. The clues to the likely appearance of the undiscovered ore body lies in observations of geological history and the effects of the factors listed above, all of which can be observed in the rocks in the area under investigation. Beyond that, observable alteration and known mineralisation provide validation data sets for the explorer to test their ore formation models against. A process model which cannot explain observed minor mineralisation in an area which is under investigation probably does not have much predictive value for the large undiscovered ore deposit.

Use all the data you have before acquiring any more

The challenge set at the beginning of the pmd*CRC was to reduce mineral discovery costs. To do so, data acquisition directed at the wrong targets has to be reduced. While some large scale data sets are invaluable for hydrothermal ore search (e.g. gravity and magnetics), the application of expensive multiple targeting methods over excessively large areas along with over-drilling of the wrong prospects largely explains high ore discovery costs. So, the process-driven explorer needs to extract maximum value out of the existing data and rock exposures before acquiring any more. Indeed, the benefits of so much unsuccessful past exploration is that many areas are quite data rich but continue to have potential for new discoveries.

In this regard, prospectivity analysis approaches can be useful to identify empirical associations between mineralisation and geological features which can then be employed generate testable hypotheses of ore formation. Both conventional prospectivity analysis methods (Bonham Carter, 1997) and new approaches such as those developed in the ***pmd*****CRC* (Murphy et al., 2004) are valuable. Of particular importance are associations in the data that conflict with pre-conceptions about relevant geological processes and which can stimulate changes in ideas about ore formation and strengthen the reliability of process models.

Observe for process and timing

The process-driven approach requires the geologist to focus on the timing of all relevant processes in relation to mineralisation. Thus careful attention to mineral parageneses, the sequence of structural events (especially evolution of the stress field through time), intrusion histories and permeability generation and occlusion is required.

Tools and Target Generation

The ***pmd*****CRC* has developed a new workflow for employing numerical modelling methods in mineral exploration. These methods include coupled deformation-fluid flow and reactive transport methods.

Application of deformation-fluid flow modelling to mineral targeting is described in detail by Potma et al. (2007) and a description of the new ***pmd****CRC* reactive transport modelling capability is provided by Cleverley et al. (2006).

Application of these tools to targeting involves a two step process, consisting of model validation using a relatively well known mineralised system followed by prediction of either the location or the properties of new mineralisation in areas under investigation.

Numerical modelling is also suited for testing the relative effectiveness of detection techniques, in particular geophysical methods. Geophysical forward modelling to test the relative effectiveness of different methods is typically based on ore shapes and physical properties from known deposits in an area. Ore shapes and physical properties both result from ore forming processes and can therefore be extremely variable depending on the structural and host rock environments. Thus, the standard empirical method for forward modelling ore responses can be quite erroneous in determining the reliability of specific geophysical techniques in making new discoveries. Numerical modelling methods are well suited for exploring the potential variety of viable geometries and physical properties, both through coupled deformation-fluid flow and reactive transport modelling. Valuable progress has already been made in the ***pmd****CRC* by Chopping and Cleverley (this volume) in converting reactive transport results directly into geophysical forward models.

Acknowledgements

I would like to thank all of my colleagues in the ***pmd****CRC*, and especially those in the CSIRO Computational Geoscience group, past and present, for all that they have taught me in the past 6 years that I have worked in the ***pmd****CRC* team.

References

Bonham-Carter, G. F., 1997. Geographic information systems for geoscientists: modelling with GIS. Pergamon, London.

Cleverley, J. S., Hornby, P. & Poulet, T., 2006, Reactive transport modelling in hydrothermal systems using the Gibbs minimisation approach. Geochimica et Cosmochimica Acta Supplement, 70(18), 106.

Murphy, F.C., Denwer, K., Green, G., Keele, R., Korsch, R.J. & Lees, T., 2004. Prospectivity Analysis, Tasmania: where Monsters lurk? In: McPhie, J. & McGoldrick, P., eds, Dynamic Earth: Past, Present and Future. Geological Society of Australia, Abstracts, 73, 102.

Potma, W., Roberts, P. A., Schaubs, P. M., Sheldon, H. A., Zhang, Y, Hobbs, B. E. & Ord, A., 2008. Predictive targeting in Australian orogenic-gold systems at the deposit to district scale using numerical modelling. Australian Journal of Earth Sciences., 55, 101-122.

Price GP & Stoker, P., 2002. Australian Geodynamics Cooperative Research Centre's integrated research program delivers a new minerals exploration strategy for industry. Australian Journal of Earth Sciences, 49, 595–600.

Sources and Reservoirs: Computer simulation of possible fluid sources and pathways in Yilgarn Au systems

HEATHER A. SHELDON AND YANHUA ZHANG

*pmd**CRC, CSIRO Exploration & Mining, PO Box 1130, Bentley, WA 6102, Australia
Heather.Sheldon@csiro.au

Introduction

The sources of fluids involved in Archaean gold mineralisation have been widely debated in the literature (e.g., Groves & Phillips, 1987; Witt et al., 1997; Walshe et al., 2006; Cleverley et al., 2007; Halley, 2007). Recent petrographic work and fluid inclusion studies have produced compelling evidence for the involvement of three chemically distinct fluids in Yilgarn gold mineralisation, described as an ambient hydrous fluid (e.g. metamorphic fluid), an oxidised magmatic fluid, and a reduced fluid that may have come from the mantle or from a basinal source (Walshe et al., 2006; Cleverley et al., 2007; Halley, 2007). Mapping of redox gradients indicates that gold deposits tend to be associated with boundaries between oxidised and reduced fluid domains, suggesting that fluid mixing was the primary deposition mechanism (Neumayr et al., 2007). These observations contradict earlier models in which a regional metamorphic fluid was envisaged as the primary transporter of gold, with deposition being attributed to fluid-rock reaction or flow through temperature gradients (e.g. Groves & Phillips, 1987; Witt et al., 1997).

The close spatial association between gold deposits and major crustal-penetrating shear zones suggests that these structures were important fluid pathways, potentially transporting fluids from the lower crust and upper mantle to interact with other fluids at shallower depths. In detail, deposits tend to be hosted by low-displacement, second or third-order structures within a few kilometres of these major shear zones (Groves et al., 1998; Cox et al., 2001), often in close proximity to granitic intrusions or porphyries. Many deposits are located close to the unconformity between late basins and underlying greenstones (Hall, 2007); this relationship could indicate that the basins acted as a fluid source, and/or that they had an influence on fluid pathways (e.g. acting as a seal) (Halley, 2007; Zhang et al., 2007b).

Numerical models can be used to explore the interactions between various fluid sources and pathways, and to quantify the fluid volumes and rates of fluid production from each source. Recent advances in numerical modelling capability enable us to simulate the coupling between magmatic and metamorphic fluid production, deformation, heat transport and fluid flow. Some examples are described below.

Approach to Modelling

FLAC3D version 3.0 (Itasca Consulting Group, 2005) provides capability to simulate fluid flow driven by deformation, thermal effects (expansion and buoyancy) and fluid production, but the user must write their own algorithms to control parameter values and the rates of processes. For example, the rate of metamorphic fluid production is determined by the rate of heating and the variation in bound water content of the appropriate mineralogy with temperature. Algorithms for simulating metamorphic and magmatic fluid production and corresponding porosity and permeability evolution in FLAC3D

were developed in the M9 project of the predictive mineral discovery Cooperative Research Centre (*pmd***CRC*), and have been applied to scenarios representing aspects of gold mineralisation in the Eastern Goldfield Superterrane (EGST) of the Yilgarn Craton (Sheldon et al., 2008).

Examples

Magmatic and metamorphic fluid production in a column of crust

Widespread emplacement of high-Ca granitic magma in the EGST at ~2685-2665 Ma would have driven regional metamorphism of the overlying basalts and sedimentary rocks (Goscombe et al., 2007). We represent this scenario with a crustal column consisting of a 5 km layer of hot granitic magma underlying 15 km of basalt (Figure 1A). The magma releases 7 wt% water (representing magmatic volatiles) as it cools from 1000 to 600 °C, and the overlying basalt releases 4 wt% water (representing dehydration reactions) as it is heated between 200 and 700 °C. Figure 1B shows the time-integrated fluid flux versus depth due to magmatic and metamorphic fluid production, and Figure 1C shows the evolution of fluid flux with time at 12 km depth. These results reveal the following important points:

- The fluid flux due to magmatic and metamorphic fluid production is very small (maximum ~10^{-11} $m^3/m^2/s$, which is 2 to 3 orders of magnitude smaller than typical fluid fluxes due to deformation or topographic head).
- Metamorphic fluid is produced and escapes from the crust within ~2 m.y. Given that most mineralisation in the EGST occurred ~10 to 20 m.y. later than the metamorphic event associated with high-Ca magmatism (Goscombe et al., 2007), this result suggests that metamorphic fluids from this event were not involved in gold mineralisation unless some other process caused these fluids to be trapped in the crust (see below).
- The 5 km layer of granitic magma releases ~3.3 times more fluid than the 15 km column of basalt.
- The time-integrated fluid flux due to regional metamorphism is ~1000 times too small to account for gold mineralisation (c.f. Cox, 1999). Hence, the fluid must be focused in order to form an economic deposit.

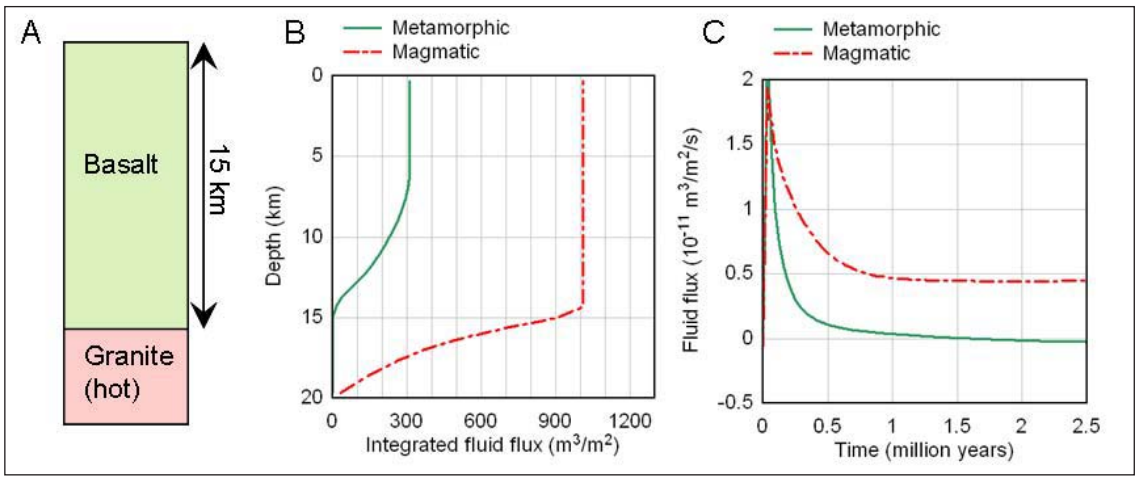

Figure 1. Magmatic and metamorphic fluid production in a crustal column. (A) Model geometry. Granite is initialised at 900 °C and allowed to cool. (B) Time-integrated fluid flux after 6.5 m.y. (C) Evolution of fluid flux at 12 km depth.

Figure 2. (opposite page) Metamorphic fluid production and focusing. (A) Geometry. Fault and conglomerate have high permeability, shale has low permeability. (B) Fluid particle tracks. (C) Time-integrated fluid flux after 1 m.y. (maximum = 1.7 x 10^4 m^3 m^{-2} s^{-1}).

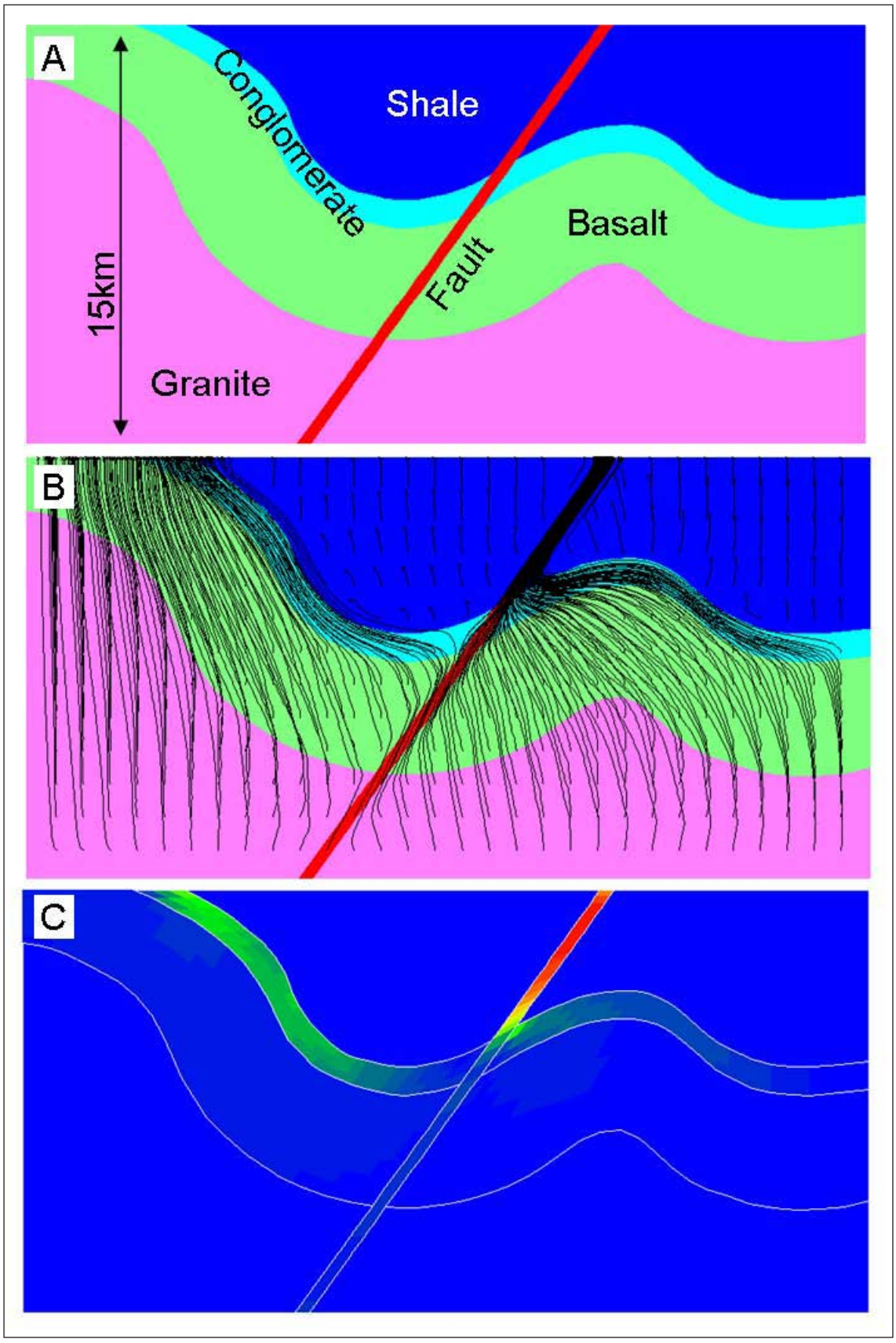

Figure 2

Fluid focusing

We investigate fluid focusing using a model representing domed granite-greenstone basement overlain by a late basin and cut by a permeable fault (Figure 2A). The basin is filled with a conglomerate which has relatively high permeability, and a shale unit which acts as a seal due to its low permeability. Metamorphic fluid production is driven by heating at the base of the model. Figure 2B shows fluid flow trajectories represented by fluid particle tracks and Figure 2C illustrates the time-integrated fluid flux after 1 million years of metamorphic fluid production. Fluid has been focused through the fault and, to a lesser extent, the conglomerate unit. The maximum integrated flux in the fault is still ~10 times too small to account for gold mineralisation, based on the estimate of Cox (1999), but the required flux could be achieved by making the fault 10 times narrower (i.e. reducing its width from 500 m to 50 m). These results indicate that metamorphic fluids could account for gold mineralisation if sufficiently focused, however the issue of timing, noted above, remains.

The fault in Figure 2 was assumed to have high permeability, but in reality fault permeability varies with time depending on the deformation regime. 3D models representing realistic fault architectures can be used to determine which faults would have been active, and therefore likely to have acted as fluid focusing pathways, under given deformation regimes. For example, a simplified representation of the 3D fault architecture in the Laverton region of the Yilgarn Craton has been used to determine the effect of varying the compression direction on fault reactivation at Wallaby and Sunrise Dam (Zhang et al., 2007a). The results were consistent with field observations which indicate dextral reactivation at Sunrise and sinistral reactivation at Wallaby.

Extension and inversion: Mixing deep and shallow fluids

The geodynamic history of the EGST includes periods of shortening, extension and strike-slip deformation (Blewett & Czarnota, 2007). The effect of different deformation regimes on fluid flow is illustrated in Figure 3, which shows fluid particle tracks due to metamorphic fluid production coupled with extension (Figure 3A) followed by shortening (representing basin inversion; Figure 3B). Extensional deformation creates space which allows the metamorphic fluid to be retained in the crust. Metamorphic fluid and surface-derived fluids converge towards the fault and a dilatant shear zone which has formed on the margin of the granite dome (Figure 3C). Thus, extension provides opportunities for mixing shallow and deep-sourced fluids. Compressional basin inversion remobilises the mixed fluids upwards (Figure 3B). Note that it is difficult to extract fluid from the shale (due to its low permeability), making it unlikely that this is the source of the reduced fluid signature in the EGST (c.f. Halley, 2007).

Effects of intrusions

Widespread emplacement of high-Ca granitic magma was followed by more localised emplacement of mafic and low-Ca granitic magmas at shallower depths. In addition to producing magmatic volatiles and driving metamorphism in the surrounding rocks, these intrusions would have caused local deformation and changes in the local stress regime, with consequent effects on fluid pathways and permeability. These effects are explored using the geometry shown in Figure 2, with the addition of two bodies representing granitic intrusions within the granite basement.

Figure 4 shows fluid particle tracks due to fluid flow driven by the release of magmatic volatiles from the intrusions. Overpressure generated by fluid production and thermal expansion drives fluids out and away from the intrusions, overriding convection in the early stages. The fluids become focused into permeable pathways, providing opportunities for fluid mixing as fluids from different sources converge.

Figure 3. (opposite page) Patterns of fluid flow due to metamorphic fluid production coupled with deformation. Geometry as in Figure 2A. (A) and (B) show fluid particle tracks during horizontal extension and shortening. (C) Fluid particle tracks and shear strain during extension. Note fluid moving towards dilatant shear zone on margin of granite dome.

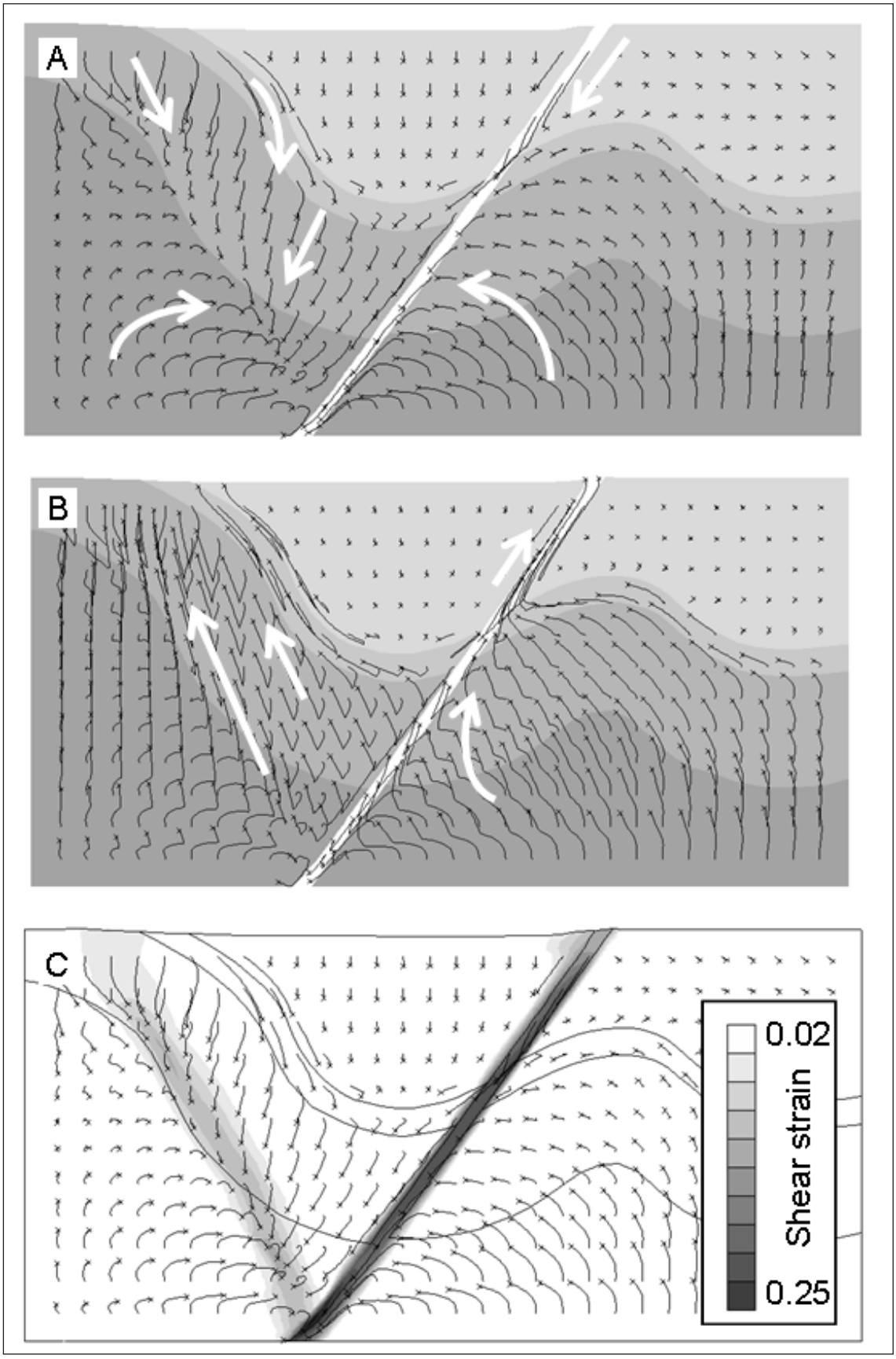

Figure 3

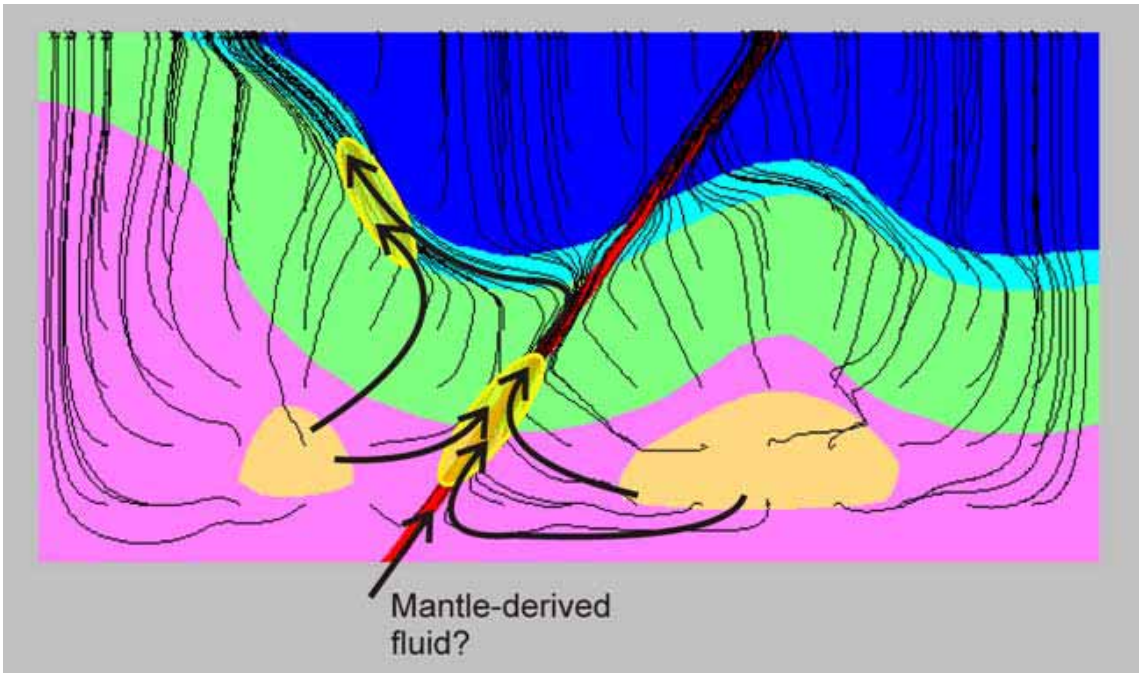

Figure 4. Fluid particle tracks due to magmatic fluid production. Shaded areas within basement represent granitic intrusions. Yellow shaded areas indicate locations of fluid mixing. Fluid coming up the fault could be derived from the mantle of lower crust.

Positive feedback between fluid flow, heat transport, permeability enhancement and metamorphic fluid production creates permeable pathways emanating from the flanks of the intrusions (Figure 5). Permeability in these regions is likely to have a preferred orientation governed by the stress regime. The effect of the intrusions on the stress regime is illustrated in Figure 6, which shows the orientation of the σ_1-σ_2 plane (representing the orientation of extension veins) in and around the intrusions. Note the chaotic pattern in and around the areas of permeability enhancement (c.f. Figure 5). This result indicates that vein orientations around intrusions are unlikely to be representative of the regional stress regime.

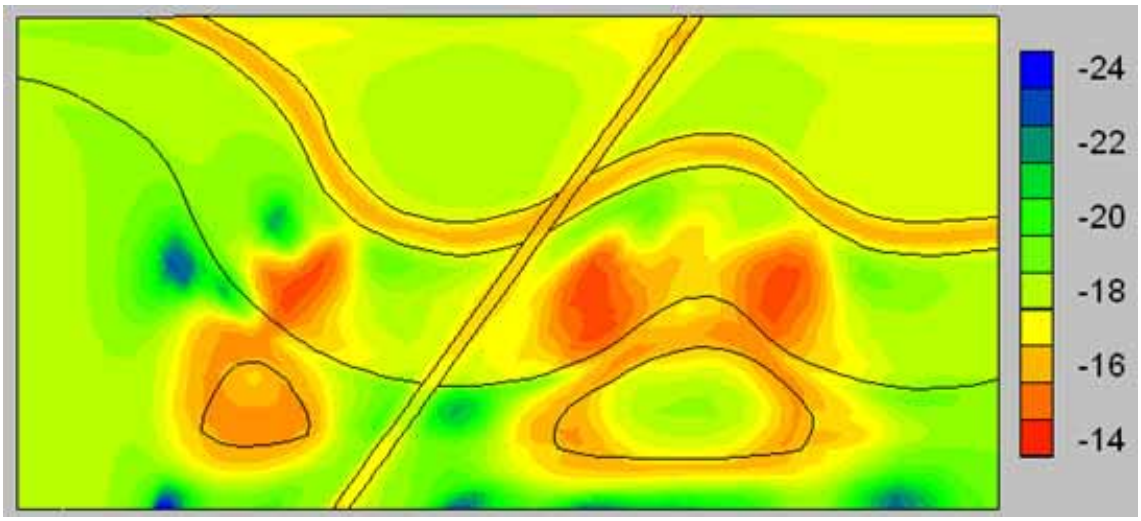

Figure 5. Permeability enhancement due to metamorphic fluid production (scale = log m2). Feedback between fluid flow, heat transport and fluid production creates plumes of enhanced permeability emanating from flanks of intrusions.

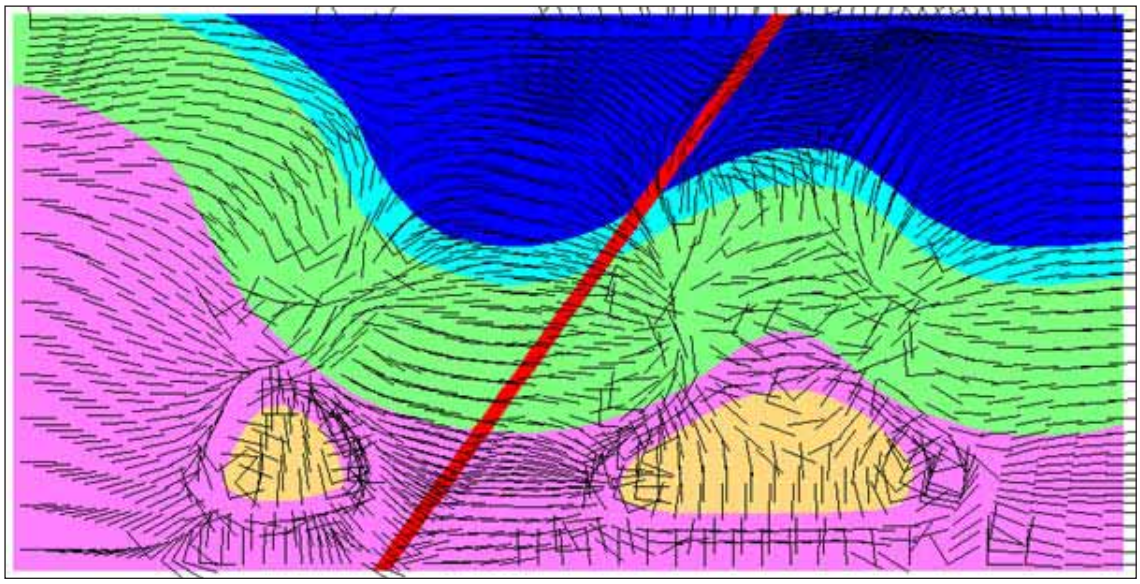

Figure 6. Orientation of the σ_1-σ_2 plane (representing extension veins) due to magmatic and metamorphic fluid production.

Conclusions

Key results from the models described above can be summarised as follows:

- Fluid flow rates due to metamorphic and magmatic fluid production are very slow.
- Magmatic volatiles are produced in greater volumes than metamorphic fluids.
- Metamorphic and magmatic fluids must be focused for mineralisation. This can be achieved in narrow fault zones. Different faults would have acted as fluid pathways at different times due to variations in the deformation regime.
- Metamorphic fluids are produced and escape from the crust within ~2 m.y. of the start of a thermal event, unless they are trapped during extensional deformation. Given that the major regional metamorphic event in the EGST was associated with contraction, and that this occurred 10-20 m.y. before gold deposition, we conclude that metamorphic fluids did not play an important role in Yilgarn gold mineralisation.
- It is difficult to extract fluids from low-permeability sedimentary units; hence it seems more likely that the reduced fluid signature of the Yilgarn represents a mantle-derived fluid (transported through the crust as a volatile phase or in magma) rather than a basin-derived fluid.
- Extension provides opportunities for mixing shallow and deep-sourced fluids.
- Fluid focusing also provides opportunities for mixing; for example, magmatic volatiles released from shallow intrusions could mix with deep crustal or mantle-derived fluid passing through a permeable fault zone.
- Intrusions result in local rotation of the principal stresses, hence vein orientations around intrusions may not reflect the regional stress regime.

References

Blewett, R.S. & Czarnota, K., 2007. Diversity of structurally controlled gold through time and space of the central Eastern Goldfields Superterrane - a field guide. Geological Survey of Western Australia, Record, 2007/19, 65pp.

Cleverley, J.S., Walshe, J.L. & Nugus, M., 2007. Tracing deep fluid sources in gold deposits of the Eastern Goldfields. In: Bierlein, F.P. & Knox-Robinson, C.M., eds, Proceedings of Kalgoorlie '07 Conference. Geoscience Australia, Record, 2007/14, 133-137.

Cox, S.F., 1999. Deformational controls on the dynamics of fluid flow in mesothermal gold systems. In: McCaffrey, K.J.W., Lonergan, L. & Wilkinson, J.J., eds, Fractures, fluid flow and mineralization. Geological Society of London, Special Publications, 155, 123-140.

Cox, S.F., Knackstedt, M.A. & Braun, J., 2001. Principles of structural control on permeability and fluid flow in hydrothermal systems. Reviews in Economic Geology, 14, 1-24.

Goscombe, B., Blewett, R.S., Czarnota, K., Maas, R. & Groenewald, B.A., 2007. Broad thermo-barometric evolution of the Eastern Goldfields Superterrane. In: Bierlein, F.P. & Knox-Robinson, C.M., eds, Proceedings of Kalgoorlie '07 Conference. Geoscience Australia, Record, 2007/14, 33-38.

Groves, D.I., Goldfarb, R.J., Gebre-Mariam, M., Hagemann, S.G. & Robert, F., 1998. Orogenic Gold Deposits: a Proposed Classification in the Context of Their Crustal Distribution and Relationship to Other Gold Deposit Types. Ore Geology Reviews, 13, 7-27.

Groves, D.I. & Phillips, G.N., 1987. The genesis and tectonic control on Archaean gold deposits of the Western Australian Shield: a metamorphic-replacement model. Ore Geology Reviews, 2, 287-322.

Hall, G.C., 2007. Exploration success in the Yilgarn craton: Insights from the Placer Dome experience - the need for integrated research. In: Bierlein, F.P. & Knox-Robinson, C.M., eds, Proceedings of Kalgoorlie '07 Conference. Geoscience Australia, Record, 2007/14, 199-202.

Halley, S., 2007. Mineral mapping: How it can help us explore in the Yilgarn Craton. In: Bierlein, F.P. & Knox-Robinson, C.M., eds, Proceedings of Kalgoorlie '07 Conference. Geoscience Australia, Record, 2007/14, 143-144.

Itasca Consulting Group, 2005. FLAC3D: Fast Lagrangian Analysis of Continua in 3 dimensions. Itasca, Minneapolis.

Neumayr, P., Walshe, J.L., Petersen, K., Young, C., Roache, A. & Halley, S., 2007. Redox boundaries in gold deposits of the Eastern Goldfields, Yilgarn, WA - Mapping a critical genetic parameter? In: Bierlein, F.P. & Knox-Robinson, C.M., eds, Proceedings of Kalgoorlie '07 Conference. Geoscience Australia, Record, 2007/14, 176-180.

Sheldon, H.A., Zhang, Y. & Ord, A., 2008. Archaean gold mineralisation in the Eastern Yilgarn: Insights from numerical models. In: Concepts to targets: A scale-integrated mineral systems study of the Eastern Yilgarn Craton. Final report of the ***pmd****CRC* Y4 project, ***pmd****CRC*, in preparation.

Walshe, J.L., Neumayr, P., Petersen, K.J., Young, C. & Roache, A., 2006. Scale-integrated, architectural and geodynamic controls on alteration and geochemistry of gold systems in the Eastern Goldfields Province, Yilgarn Craton. MERIWA Report, Perth, 287 pp.

Witt, W.K., Knight, J.T. and Mikucki, E.J., 1997. A synmetamorphic lateral fluid flow model for gold mineralization in the Archean Southern Kalgoorlie and Norseman Terranes, Western Australia. Economic Geology, 92, 407-437.

Zhang, Y., Schhaubs, P.M., Henson, P.A., Czarnota, K., Ord, A., Sheldon, H.A. & Blewett, R.S., 2007a. Laverton regional numerical model: Understanding strain localisation. In: Bierlein, F.P. & Knox-Robinson, C.M., eds, Proceedings of Kalgoorlie '07 Conference. Geoscience Australia, Record, 2007/14, 248.

Zhang, Y., Sheldon, H.A., Blewett, R.S., Ord, A., Barnicoat, A.C. & Czarnota, K., 2007b. Deformation and fluid flow associated with late basins and domes: Implications for mineralization in the Yilgarn. In: Bierlein, F.P. & Knox-Robinson, C.M., eds, Proceedings of Kalgoorlie '07 Conference. Geoscience Australia, Record, 2007/14, 249.

Flowpaths and Drivers: New spectral methods and products for resource and surface materials mapping in Queensland, Australia - methods and applications for industry

MATILDA THOMAS[1], CARSTEN LAUKAMP[2], THOMAS CUDAHY[3] AND MAL JONES[4]

[1]*pmd***CRC*, Geoscience Australia, GPO Box 378, Canberra, ACT 2601
[2]*pmd***CRC*, James Cook University, Townsville, QLD 4811
[3]CSIRO Exploration and Mining, Australian Resources Research Centre, PO Box 1130, Bentley, WA 6102
[4]Geological Survey of Queensland, 80 Meiers Road, Indooroopilly, QLD 4068
Matilda.Thomas@ga.gov.au

Spectral geology is increasingly recognised as an effective method of mapping both mineral occurrence and composition for a wide range of applications. For explorers, new advances in spectral processing and data delivery mean that spectral methods are more accessible and easier to integrate with other datasets, making for simpler, more efficient interpretation. As spectral data becomes more widely available, industry has access to cutting-edge techniques for their exploration programs, with some unexpected benefits such as outcrop identification. Spectral techniques are also providing beneficial new tools for understanding the often complex relationship of surface materials which can impede mineral exploration.

The *pmd***CRC* has been involved in spectral work for the Mt Isa (I7) and Fluids (F6) projects and has been furthering and advancing earlier work by van der Wielen et al. (2005). An additional project – the I7 Hydrothermal Footprints project was started 2006, in conjunction with the Smart Exploration Program of the Queensland State Government, as part of a joint venture to collect and process new hyperspectral data in Queensland. This project was also designed to calibrate the pre-existing Advanced Spaceborne Thermal Emission and Reflective Radiometer (ASTER) satellite mosaic of van der Wielen et al. (2005) and to develop new techniques and software to improve the products that could be obtained from the existing ASTER dataset available from Geoscience Australia.

The ASTER sensor is housed on board Terra, the Earth Observing System (EOS) satellite. It is a multispectral imaging device that records data in 14 spectral bands; 3 bands in Visible Near-Infrared (VNIR) with 15 metre spatial resolution, 6 bands in Short Wave Infrared (SWIR) with 30 metre spatial resolution and 5 bands in Thermal Infrared (TIR) with 90 metre spatial resolution. For geological purposes the VNIR and SWIR wavelengths are best for identifying and mapping alteration associated with Mineral Systems, as those spectral regions contain the most diagnostic absorption features for important minerals and mineral groups, such as ferric and ferrous minerals, and AlOH and MgOH group minerals. Both ASTER and HyMap (a 128 band hyperspectral airborne instrument with ~4-8m spatial resolution) are

reflectance spectroscopy methods, using light from the sun reflected from the ground surface that is captured and recorded by sensors.

The original Mt Isa ASTER mosaic includes over 130 scenes tiled together (probably the largest ASTER mosaic to date), processed using ER-Mapper software to produce a number of geology/mineral products (van der Wielen et al., 2005). For the I7 Mount Isa Footprints project, new processing methods were used, including most importantly calibration with the high spatial and spectral resolution HyMap hyperspectral data. Software tools were developed to improve and simplify corrections and masking of the dataset.

New software processing tools, built by CSIRO as ENVI software add-ons, were used to process the new HyMap and ASTER respectively in the Mt Isa region (see Figure 1 for ASTER and HyMap coverage). The re-calibrated and reprocessed data has been provided as a series of products in a GIS compatible format which is easy to use and integrate with other data, allowing for quick comparison and analysis. This means increased interpretability and eases use by non-expert users and should lead to greater uptake by the exploration community. Spectral products, when combined with other chemical and structural information, are in particular relevant in the location and mapping of hydrothermal systems. In several test cases in Western Australia, spectral techniques have been used to successfully identify alteration patterns and regional chemistry (Cudahy et al., 2005). By providing the processed data products and user-notes free of charge, over the web, the Mt Isa work encourages new users to see spectral products as part of the suite of tools available for use in exploration alongside standards such as surface geology maps, gravity, aeromagnetic and radiometric data.

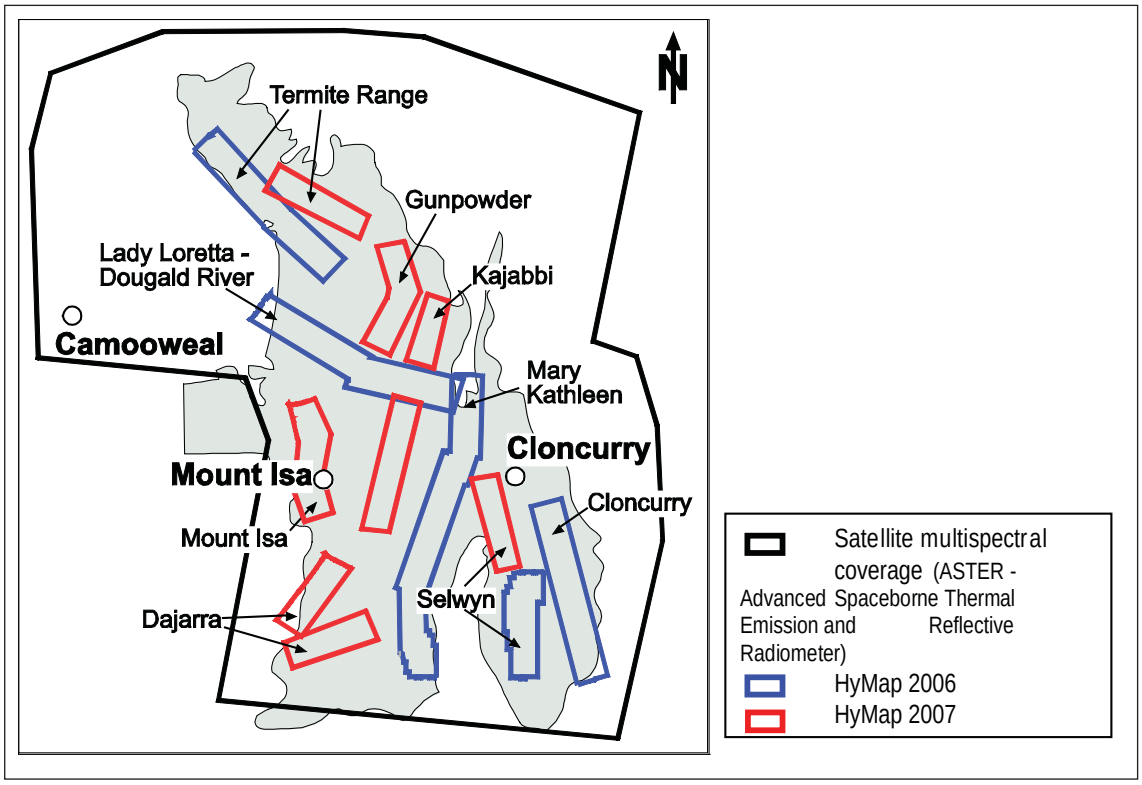

Figure 1. Coverage of ASTER and HyMap imagery over the Mount Isa inlier, Queensland, Australia. (Black outline = ASTER, Blue & Red boxes = HyMap swaths, Grey shaded area = approximate outcrop extent of the Mount Isa Inlier).

With the original 2005 ASTER products designed to be interpreted like gravity or magnetics images with a continuum of response, it proved difficult for many explorers to interpret and requests were made

for masked more reliable products that would be simpler to interpret and integrate with other datasets. The new products were aimed at increasing usability for explorers, and were planned to improve on the original products by masking and thresholding data to reduce interference from clouds, vegetation etc, or low-value (and probably unreliable) pixels. This project saw significant improvements in the processing time for mosaicing, masking and thresholding, and the new products are designed to present a more realistic surface picture. Improvements to reduce and remove interference from vegetation are continuing, but even though vegetation masks were applied, the vast changes over the time frame of the ASTER scenes means it is still the most challenging issue for ASTER processing and interpretation.

The processing steps to create the new ASTER mosaic included usual pre-processing followed by calibration with the HyMap data. The HyMap had already been ground-truthed and validated using field samples analysed with a hand-held PIMA (Portable Infrared Mineral Analyser), so was well constrained The ASTER scenes are of much lower spatial and spectral resolution and due to different scenes being collected at many different times, before after fires/droughts etc) and the scale difference makes it unsuitable for direct ground-truthing by PIMA.

A new approach to calibration was adapted, using the HyMap to validate the ASTER by selecting suitable geological targets that occurred on overlapping ASTER and HyMap scenes. The spectral response between the two instruments was compared to see if they were similar. Because the Hymap has a ~5 m pixel compared to ASTER's 15-30 m, and many more bands, the Hymap was down-sampled to match the pixel size of the ASTER, (roughly 4 HyMap pixels were averaged to make a pseudo-ASTER pixel) and it was also spectrally down-sampled to match the ASTER bands to generate a kind of 'pseudo ASTER image'. Pixels from this pseudo-image were then compared to the real ASTER data and a series of gain and offset calculations were plotted for each of the ASTER bands to see how different the information was in the 'same' pixels for the 2 datasets. Because ASTER is collected by a satellite rather than an aircraft, and collects much less 'information' than the high resolution HyMap instrument, it was expected the two products would quite different. It was thought this process would highlight the inaccuracy and ambiguity of the satellite data, but the band comparisons were surprisingly good, with all bands showing good linear correlations (Figure 2).

Errors in the results, caused largely by seasonal differences in vegetation cover (dry versus green) between the HyMap and the ASTER, proved to be the most difficult to remove, but correlations were still very good given the significant spectral and spatial resolution differences between the satellite and airborne data. The new techniques have improved the reliability and measurable accuracy of the ASTER products. The band comparison demonstrates the 2 instruments concur on spectral information and that using the HyMap to calibrate the ASTER is useful and increases the accuracy of the ASTER data.

The new products comprise a suite of the most geologically meaningful band combinations highlighting outcrop and alteration patterns. Currently, the available suite included 13 ASTER and 21 HyMap products with accompanying explanatory notes including metadata on processing and relative accuracy ratings for each product as a Word document.

The calibrated and mosaiced ASTER products, along with all the PIMA, field data and HyMap products are available at: www.em.csiro.au/NGMM for free download in JPEG2000 and ECW (high compression) formats and include the products listed in the table below. The raw HyMap data can be requested (on external hard drive) from GSQ, and ASTER scenes can be purchased from ACRES at Geoscience Australia at http://www.ga.gov.au/acres/prod_ser/asterpri.jsp.

Most of these products are helpful in understanding and mapping mineralisation and identifying flow paths in the landscape. In combination with existing geological maps, ASTER can be helpful in following regional trends and picking up significant chemical changes, often showing up structural boundaries such as unconformities and faults by identifying mineral group changes on the surface.

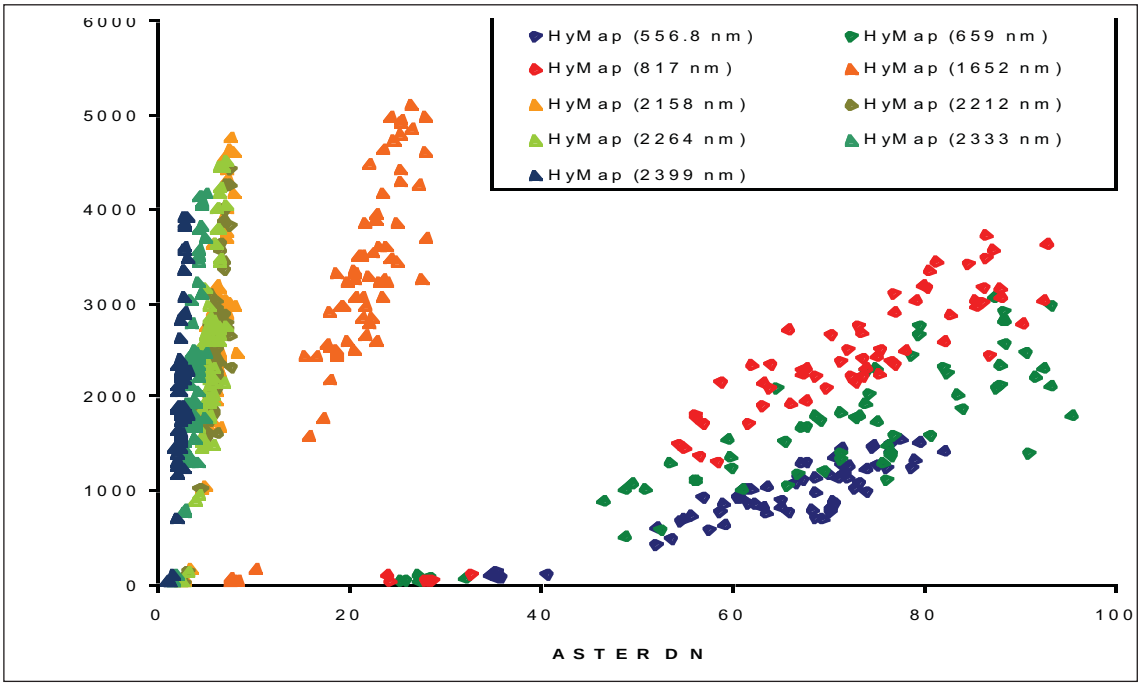

Figure 2. Pixel comparison for the overlapping ASTER and downsampled HyMap reflectance bands, showing good correlations in all bands.

Although ASTER and HyMap can only map materials in the top few millimetres, expression of underlying materials is quite clear in several products. The HyMap have proved to be much better at delineating more subtle chemical signatures, and finding new outcrops with its ~5 m resolution. However, ASTER still provides useful, regional-scale information. One ASTER product that has proved to be significant for the mapping of important dark shale units is the ASTER 'opaques' product, which is good for delineating dark lithologies that often host ore in the Mt Isa inlier.

For mineral exploration purposes, ASTER is most suited to look for mineralogical changes and identify areas of high contrast in the various products to target things such as redox boundaries (e.g., Laukamp et al., 2008). ASTER can highlight regions of interest, also by mapping contrast boundaries, but not to the same detail or mineral type accuracy as HyMap, but is still useful for identifying areas of interest for more detailed follow-up work. Despite the high degree of calibration and attention to processing, ASTER is still only a regional tool, but when used in combination with other information, is still capable of providing detailed mineralogical information, its main strengths being regional coverage and low cost relative to HyMap.

The CSIRO regolith product is a band combination that enhances iron and clay weathering products, often mapping out channels and different materials in channels. This product appears to provide some relative indication of age of different channel sediments, by delineating crosscutting relationships and also by channel clay vs. iron oxide materials, but will need further work to verify this. The regolith product has a moderate accuracy as it is complicated by mixing with vegetation as well as any residual additive effects (e.g., aerosol scattering in the VNIR) and ASTER instrument crosstalk effects in the SWIR bands). It does however provide important context information and indicate some areas of transported and in situ sediments.

Although the ASTER products have not been systematically ground-truthed, it is hoped the new products will make it easier for industry user in integrate with their existing datasets, and it is anticipated new

ASTER products:		HyMap products:	
1.	False colour basemap	1.	Natural colour basemap
2.	Green vegetation content	2.	False colour basemap;
3.	CSIRO's regolith ratios	3.	Green vegetation content
4.	Iron oxide content	4.	Dry vegetation content
5.	Ferrous iron	5.	Iron oxide content
6.	AlOH (muscovite, kaolinite, Al-smectite) content	6.	Ferrous iron
7.	AlOH (muscovite, kaolinite, Al-smectite) composition	7.	Kaolin content
8.	advanced argillic (alunite, pyrophyllite, kaolinite)	8.	Kaolin crystallinity
9.	FeOH (chlorite, epidote) content	9.	Al-smectite content
10.	MgOH content; (calcite/dolomite/chlorite/epidote/amphibole)	10.	Al-smectite composition
11.	MgOH composition; (calcite/dolomite/chlorite/epidote/amphibole)	11.	White mica (paragonite-muscovite-phengite) content
12.	Ferric iron and MgOH	12.	White mica composition
13.	Ferrous iron and MgOH	13.	White mica crystallinity
		14.	MgOH content; (calcite/dolomite/chlorite/epidote/amphibole)
		15.	MgOH (as above) composition
		16.	Ferris iron and MgOH
		17.	Ferrous iron and MgOH
		18.	Amphibole-chlorite content
		19.	Epidote content
		20.	Opaques
		21.	Hydrated silica

**NB. ALL of these products have varying degrees of accuracy and can be affected by vegetation changes such as fire scars, seasonal change etc and interference from other minerals and materials. It is important to read and use the accompanying PRODUCT DESCRIPTIONS provided on the online data-download page.*

application will be found as more people start to use the images. Applications for mineral exploration have currently focused on regional indicators, using AlOH group products, particularly the content products for detecting regions containing illite, muscovite, Al-smectite, kaolinite, which does suffer interference from vegetation, but has a moderate degree of accuracy. The AlOH group product also is subject to some interference from vegetation and other effects, but cross-checking with HyMap or other mineralogical data where available can inform and improve interpretation in new areas (Figure 3).

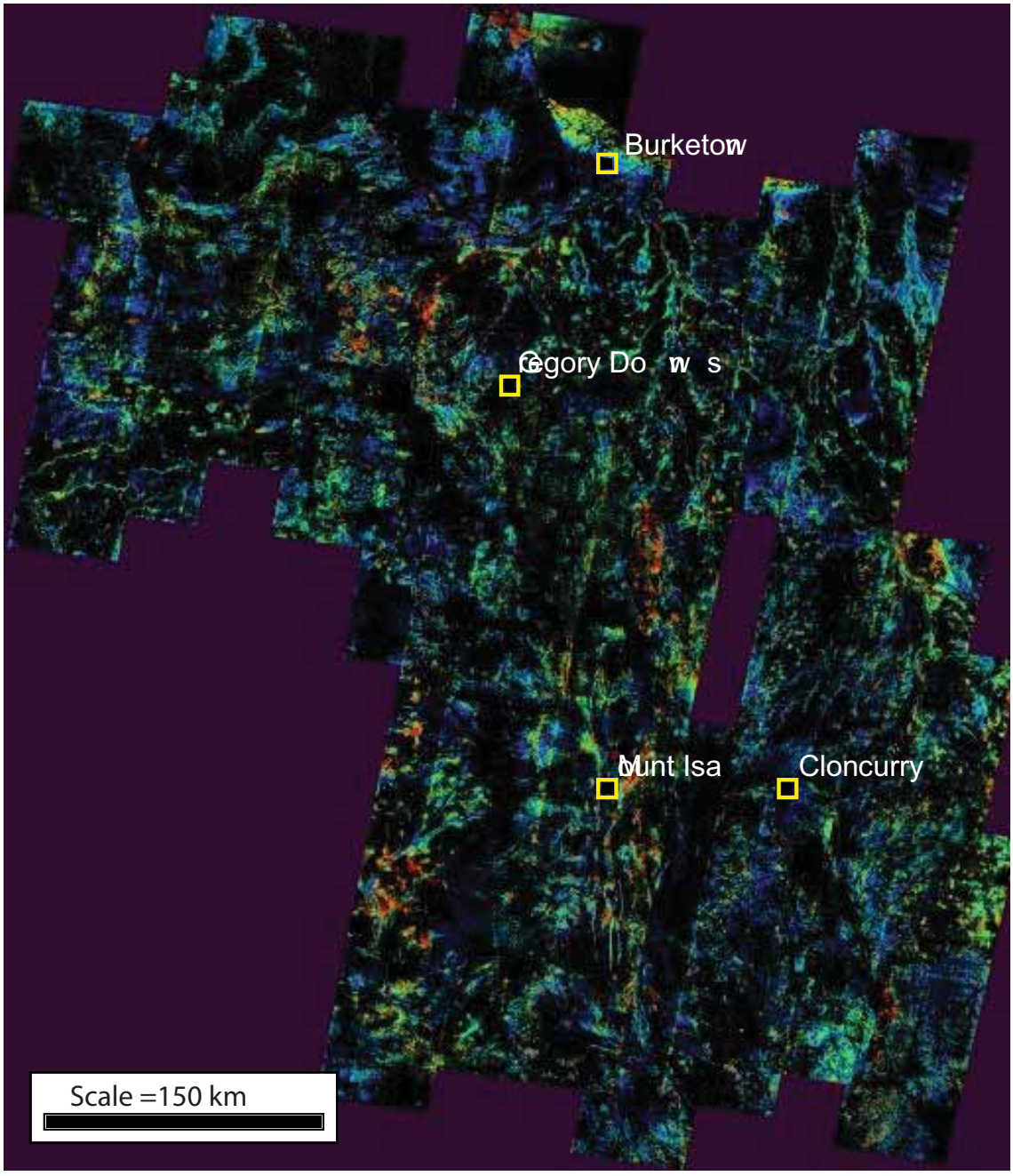

Figure 3. ASTER mosaic – Al-clay content product; RED: high Al-clay mineral content, BLUE: low content, black: below threshold or masked from dataset.

References

Cudahy, T.J., Caccetta, M., Cornelius, A., Hewson, R.D., Wells, M., Skwarnecki, M., Halley, S., Hausknecht, P., Mason, P. & Quigley, M.A., 2005. Regolith geology and alteration mineral maps from new generation airborne and satellite remote sensing technologies and Explanatory Notes for the Kalgoorlie-Kanowna 1:100,000 scale map sheet, remote sensing mineral maps. MERIWA Report No. 252, 114pp.

Laukamp, C., Cudahy, T., Thomas, M., Jones, M., Cleverley, J.S. & Oliver, N.H.S., 2008. Recognition of hydrothermal footprints in the Eastern Fold Belt of the Mount Isa Inlier using geophysical-geochemical spatial data. ***pmd***CRC* Project 17, Final Report, in preparation.

van der Wielen, S.E., Oliver, S., Kalinowski, A.A. & Creasy, J., 2005. Remotely sensed imaging of hydrothermal footprints in Western Succession, Mount Isa Inlier. In: Gibson, G.M. & Hitchman, A., eds, Project 11 – Western Succession basin architecture and ore systems. ***pmd***CRC* 11 Project Final Report, pp 177-185, http://www.pmdcrc.com.au/final_reports_project11.html

Sources and Reservoirs: Stable isotopes and mineralogy as indicators fluid source

JOHN WALSHE[1], PETER NEUMAYR[2], KLAUS PETERSEN[2], JANET TUNJIC[3], SCOTT HALLEY[4] AND JAMES CLEVERLEY[1]

[1]*pmd***CRC*, CSIRO Exploration & Mining, Bentley, PO Box 1130, Bentley, WA 6102
[2]*pmd***CRC*, School of Earth and Geographical Sciences, University of Western Australia, 35 Stirling Highway, Crawley, WA 6009
[3]St Ives Gold Mining Company (Pty) Limited, PO Box 359, Kambalda West, WA 6444
[4]Mineral Mapping Pty Ltd, 24 Webb St, Rossmoyne, WA 6148
John.Walshe@csiro.au

Introduction

Questions of the nature and location of the salient fluid reservoirs for hydrothermal systems and the timing of fluid release are long standing. The difficulties of storing endogenetic crustal fluids until critical times of metallogenesis are well canvassed in the literature. Over the last several decades, the geophysical community has been progressively developing a picture of deep ancient architectures in major provinces that invites the question: are the salient fluids are stored in the mantle rather than the crust? If this were true what would be the nature of these fluids and how could such fluids be recognised and pathways of deep-Earth fluids tracked in the crust? Studies undertaken within the ***pmd***CRC* suggest an answer in the affirmative is most likely. Salient results from studies of Eastern Goldfields, Yilgarn Craton that have contributed to an understanding of deep-Earth fluids and their role in metallogenesis are summarised here and in (Kendrick et al., 2008).

Fluid reservoirs in Archean gold deposits

Traditionally, models of formation of Archean lode Au deposits have assumed one dominant aqueous carbonic fluid (H_2O - CO_2 - NaCl ± H_2S ± CH_4 ± N_2) in the system, with the CO_2 concentration in the fluid taken as >5 mole percent (Hagemann & Cassidy, 2000; Groves et al., 2003). In these single-fluid models Au is considered to have been transported by a reduced sulfur complex in a near neutral fluid with Au deposition occurring through fluid-rock reaction or fluid boiling. It is now recognised that asymmetric, kilometre-scale alteration footprints can be identified in the Au systems of the Yilgarn Craton of Western Australia and Au mineralisation occurs preferentially within or subjacent to boundary zones between contrasting alteration domains (Neumayr et al., 2003, 2005, 2008; Walshe et al., 2003: Halley, 2007). It is difficult to reconcile these large-scale, mineralogical and geochemical dispersion patterns with single fluid mineralisation models. Here, it is argued that multiple-fluid models are required to explain the diversity of mineral alteration assemblages and patterns of mineral zoning at district to deposit scale. It is argued that it was the interplay between chemically contrasting fluids and host rocks that sustained physicochemical gradients in the system. Gradients occur in redox, pH, as well as in the activity of S, C, Cl and water. Ultimately it was these physicochemical gradients that provided the chemical drive for gold transport and deposition in the system.

Three distinct fluid types or end-member fluids are required to explain the fluid inclusion, mineralogical and isotopic constraints as well as the asymmetry of the district to deposit -scale alteration in lode Au deposits of the Eastern Goldfields, Yilgarn Craton. Fluid 1 is considered an ambient crustal fluid that was aqueous with low concentrations of salt and volatiles. It is likely that the major reservoirs of water, late in the metamorphic history, were in synorogenic sedimentary basins. Fluids 2 and 3 and are considered volatile-rich 'deep Earth' fluids that ultimately controlled the physicochemical gradients (redox, pH, activities of S, C, Cl) driving gold transport and deposition (Figure 1).

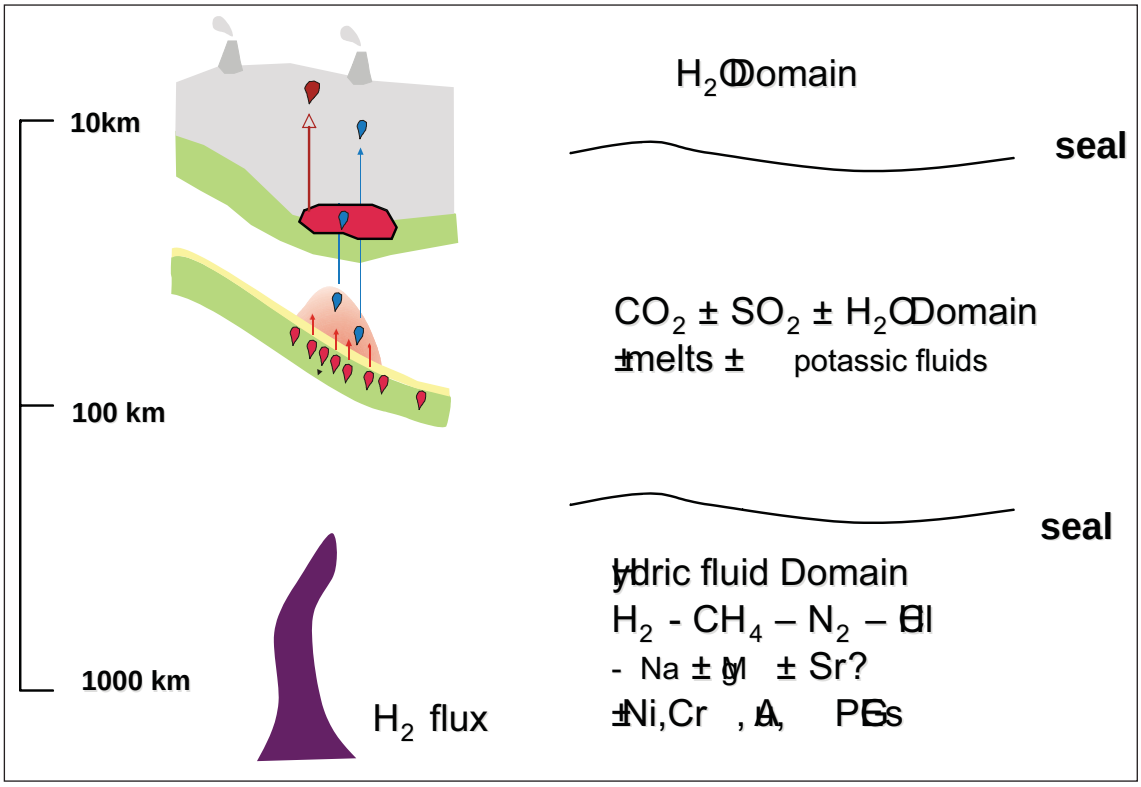

Figure 1. Illustration of deep-Earth fluid reservoirs of reduced and oxidised anhydrous fluids. Thermodynamic calculations suggest the reduced fluid (hydric fluid) was stable at depths greater than 300 to 400 km, but the ultimate source of the hydrogen may have been the Earth's core.

Tomographic studies have identified structure to depths of > 100 km, suggesting possible fluid pathways to at least depths. Fluid 2 was of magmatic affinity, dominated by CO_2 and SO_2, but with capacity to transport elements such as Te, V, Mo, Bi, W and possibly K. $\delta^{13}C$ of CO_2 is estimated at -5 to -6 ‰ and $\delta^{34}S$ of S at ~ 0 ‰, consistent with a mantle origin for CO_2 and SO_2 (Figure 2). Radiogenic Pb may have been acquired by fluids stored in crustal domes but ultimately the oxidised magmatic fluids probably originated from melting of metasomatised upper mantle. Fluid 3 was a highly reduced CH_4 - N_2 - H_2 fluid that transported acid volatiles (H_2S, HCl ± HF), noble gases (Ne and Ar) of mantle origin, possibly metal hydrides (e.g. NaH, MgH_2, AlH_3 and SiH_4), and probably gold. Thermodynamic calculations suggest the reduced fluid was stable at depths greater than 300 to 400 km. Mixing of reduced and oxidised anhydrous deep-Earth fluids appears to be the salient mechanism of gold deposition in the crust. Mixing of 'deep-Earth' fluids with ambient aqueous fluids drove district-scale acidic alteration and dispersion of Au.

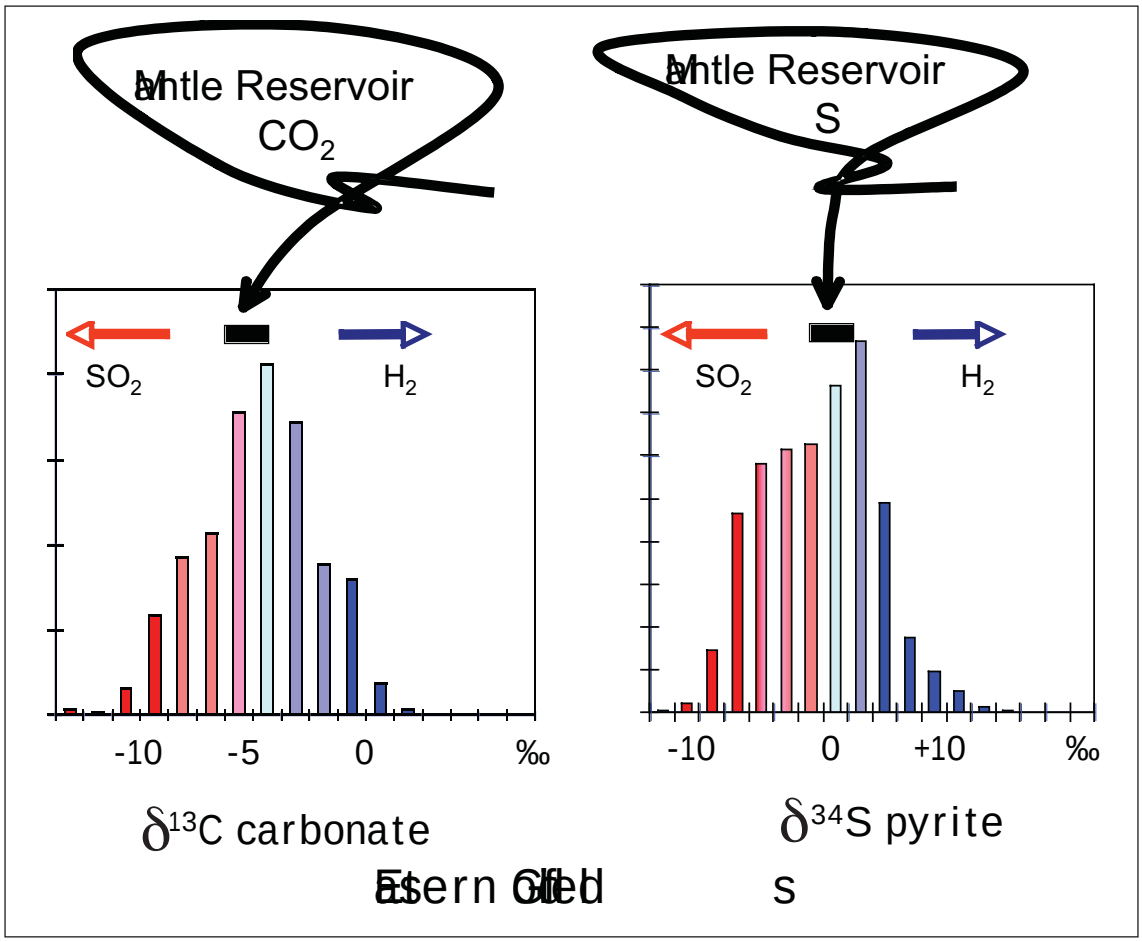

Figure 2. Histograms of $\delta^{13}C$ carbonate and $\delta^{34}S$ pyrite for the Eastern Goldfields, Yilgarn Craton. Mantle reservoirs of $\delta^{13}C$ CO_2 and $\delta^{34}S$ sulphur are indicated.

Mapping pathways of deep-Earth fluids in a mineralising system: Mount Isa

A systematic study of $\delta^{34}S$ pyrite, chalcopyrite and pyrrhotite and $\delta^{13}C$ carbonate and graphite was undertaken through the 3500 Cu orebody to look for evidence of H_2-rich fluid pathways in the lower part of the Cu-ore system, proximal to the Paroo Fault. The dominance of H_2 in the fluids may be tracked by positive departures of $\delta^{13}C$ carbonate from the dominant reservoir of $\delta^{13}C$ CO_2, reflecting the reduction of oxidised carbon species e.g. $CO_2 + 4H_2 = CH_4 + 2H_2O$. Similarly positive departures in $\delta^{13}C$ values of carbon with respect to carbonate may be taken as evidence of enhanced H_2 flux. A significant ^{13}C enrichment in carbonate, as well as in graphite, hint at a H_2 flux zone in the transition zone to the footwall of 3500 ore-body as documented in Figure 3.

Evolution of deep-Earth fluids in the crust

Isotopic studies from the Eastern Goldfields, Yilgarn Craton and the Mount Isa Inlier support the argument for the involvement of deep-Earth fluids in major mineral systems. Such fluids will be highly reactive in the crust, and are likely to drive significant changes in fluid chemistry. Such changes may or may not aid metal mobilisation and/or fixation in the crustal environment. The responses to injecting a hydric fluid, stable at > 600 km within the Earth, into crustal rocks ± aqueous crustal fluids, will depend on the precise reaction path and P/T conditions. A significant factor will be the ratio of alkali and alkali-earth halides to HF and HCl, which will control the evolution of acid/base balance of the fluids as they

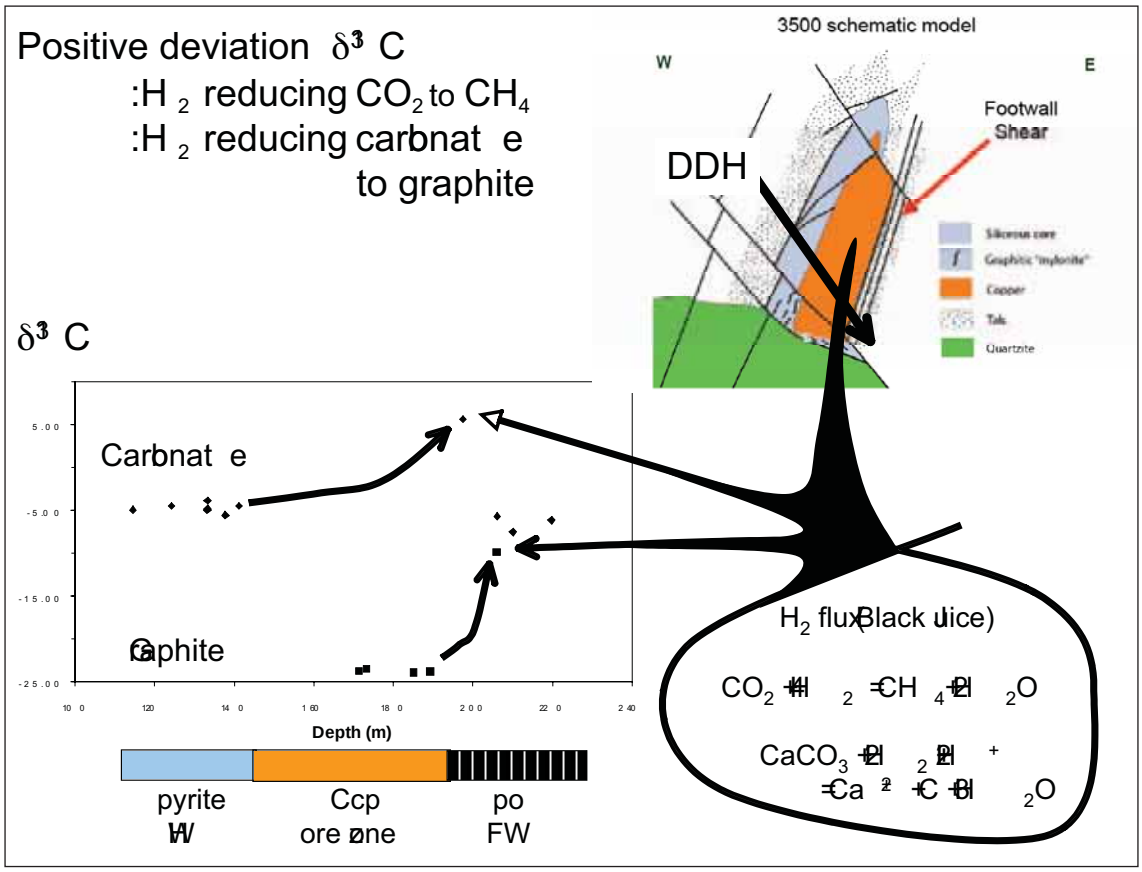

Figure 3. Tracking H_2-rich fluid pathways in the 3500 Cu orebody, Mount Isa. H_2-rich fluids pathways are denoted by ^{13}C enrichments in carbonate and carbon in the transition zone to the footwall of 3500 ore body. The ^{13}C enrichments in carbonate reflect partial reduction of oxidised carbon species to methane with the residual oxidised species being enriched in ^{13}C. The ^{13}C enrichments in carbon, such that the $\delta^{13}C$ values of carbon approach that of the carbonate, imply in-situ reduction of carbonate to carbon. Both reactions require a reductant to proceed. The most likely reductant was H_2.

react with crustal fluids and rocks degrading to aqueous fluids of varying acidity, redox state and salinity. Relatively high halogen to alkali ratios should lead to acid production through dissociation of HCl and HF in aqueous crustal fluids; assuming limited degassing of hydrogen. Loss of hydrogen through degassing, or consumption of hydrogen through reaction with oxidised species or rocks (SO_2, sulphate and carbonate or CO_2) could lead to neutral to alkaline, highly saline and sodic brines. These 'degraded' hydric fluids can explain the widespread occurrence of acidic alteration (see Figure 4) and/or district-scale albitisation in major mineral provinces and within sedimentary basins. With declining pressure, hydridic fluids are likely to evolve to $H_2 \pm CH_4 \pm H_2S \pm N_2$ gases that maintain significant reducing capacity with potential to mobilise carbonaceous material in the crust to produce sour gas and petroleum products.

Concluding remarks

It is suggested that styles of district- to terrain-scale alteration in crustal rocks, potentially related to the passage of deep-Earth fluids through the crust, could include:

- Acidic alteration assemblages (muscovite ± paragonite ± pyrophyllite), as found in Archean gold systems and in the Witwatersrand Basin
- District-scale albitic alteration (Mt Isa Inlier)
- District-scale graphitisation of faults and fractures.

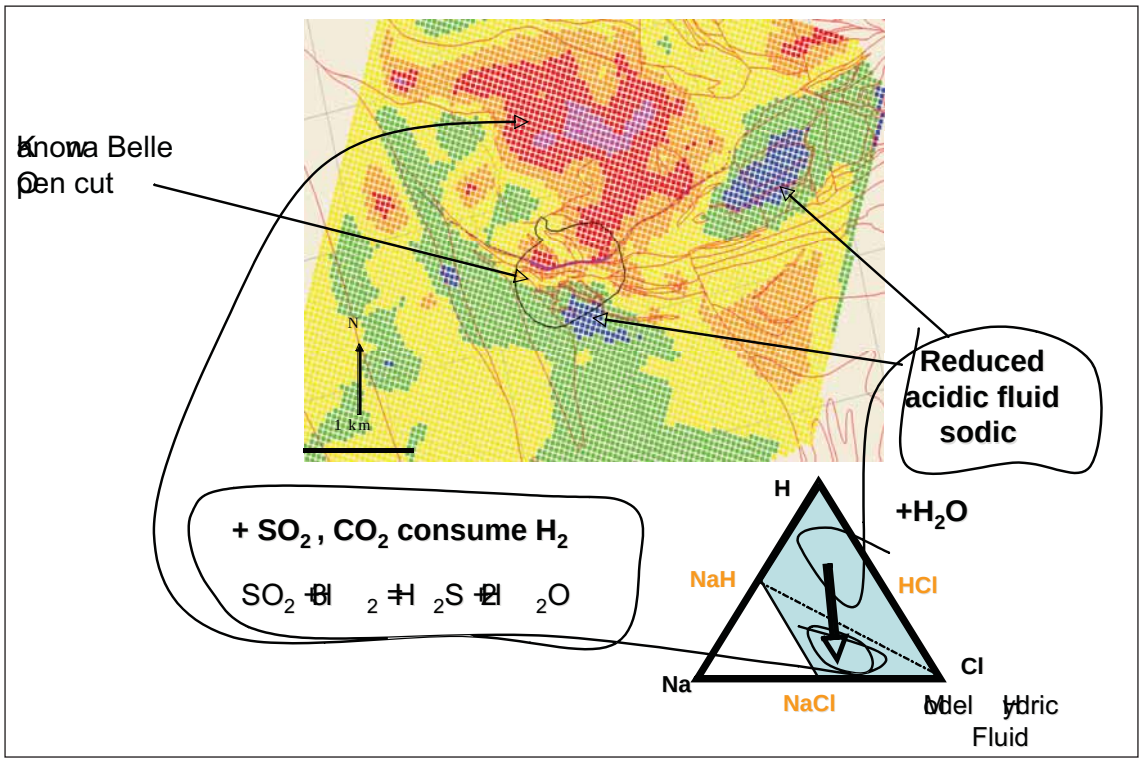

Figure 4. Mapping 'acid blooms' of hydric fluids in the Kanowna Belle district with shortwave infrared (SWIR) wavelength for AlOH in white mica (2200 nm). Cool colours: short wavelength (muscovite–paragonite) denote acidic domains. Warm colours: long wavelength (phengite) denote neutral to alkaline domains. Note the strong gradient in wavelengths across the Kanowna Belle deposit from footwall (long wavelength) to hangingwall (short wavelength). The acidic fluids result from dissociation of HCl on mixing with aqueous fluids most probably sourced from the late basins. The consumption of H_2 or H+ via, for example, the reaction with SO_2 or sulphate buffers pH to neutral-alkaline conditions.

Arguably, high reflectivity zones observed in seismic sections in the Eastern Goldfields reflect intense acid alteration. Anomalous zones of conductivity beneath the Kalgoorlie and Olympic Dam deposits, determined from magnetotelluric studies, demonstrate large domains of graphitisation in the mid- to lower-crust. Such domains may well be tracking the reaction and degradation of hydric fluids from the mantle in the crust. Transcrustal domains of graphitisation may have helped provide the chemical buffers to allow super-reduced hydric fluids to penetrate to high levels in the crust.

References

Groves, D.I., Goldfarb, R.J., Robert, F. & Hart, C.J.R., 2003. Gold deposits in metamorphic belts: Overview of current understanding, outstanding problems, future research, and exploration significance. Economic Geology, 98, 1-29.

Hagemann, S.G. & Cassidy, K.F., 2000. Archaean orogenic gold deposits. Reviews in Economic Geology, 13, 9-68.

Halley, S., 2007. Mineral mapping - how it can help us explore in the Yilgarn Craton In: Bierlein, F.P. & Knox-Robinson, C.M., eds, Proceedings of Kalgoorlie '07 Conference. Geoscience Australia, Record, 2007/14, 143-144.

Kendrick, M.A., Walshe, J.L., Mark, G., Petersen, K., Baker, T., Phillips, D., Honda, M., Oliver, N.H.S., Fisher, L.,

Gillen, D., Williams, P.J. & Fu, B., 2008. Sources and reservoirs: Noble gases as tools for constraining a mantle connection during orogenic-gold and IOCG mineralisation. pmd*CRC Plenary Conference, Perth, this volume.

Neumayr, P., Hagemann, S.G., Walshe, J. & Morrison, R.S., 2003. Camp- to deposit-scale zonation of hydrothermal alteration in the St. Ives gold camp, Yilgarn Craton, Western Australia: evidence for two fluid systems? In: Eliopoulos, D.G., ed., Mineral Exploration and Sustainable Development. Seventh Biennial SGA Meeting, Millpress, Athens, 799-802.

Neumayr, P., Petersen, K.J., Gauthier, L., Hodge, J.L., Hagemann, S.G., Walshe, J.L., Prendergast, K., Connors, K., Horn, L., Frikken, P., Roache, A. & Blewett, R.S., 2005. Mapping of hydrothermal alteration and geochemical gradients as a tool for conceptual targeting: St. Ives Gold Camp, Western Australia. In: Mao, J. & Bierlein, F.P., eds, Mineral Deposit Research: Meeting the Global Challenge, 8th Biennial SGA meeting. Springer, Berlin, Vol. 2, 1479-1482.

Neumayr, P., Walshe, J.L., Hagemann, S.G., Petersen, K., Roache, A., Frikken, P., Horn, L. & Halley, S., 2008. Oxidized and reduced mineral assemblages in greenstone belt rocks of the St. Ives gold camp, Western Australia: vectors to high- grade ore bodies in Archaean gold deposits? Mineralium Deposita, in press.

Walshe, J.L., Halley, S.W., Hall, G.A. & Kitto, P., 2003. Contrasting fluid systems, chemical gradients and controls on large-tonnage, high-grade Au deposits, Eastern Goldfields Province, Yilgarn Craton, Western Australia. In: Eliopoulos, D.G., ed., Mineral Exploration and Sustainable Development. 7th Biennial SGA Meeting. SGA, Athens, 827-830.

Deposition: Multi-fluid systems, depositional processes and targeting

JOHN WALSHE[1], PETER NEUMAYR[2], KLAUS PETERSEN[2], TONY ROACHE[3], JANET TUNJIC[4], SCOTT HALLEY[5] AND JAMES CLEVERLEY[1]

[1]*pmd***CRC*, CSIRO Exploration & Mining, Bentley, PO Box 1130, Bentley, WA 6102
[2]*pmd***CRC*, School of Earth and Geographical Sciences, University of Western Australia, 35 Stirling Highway, Crawley, WA 6009
[3]*pmd***CRC*, CSIRO, Joe Lord Core Library, PO Box 1664, Kalgoorlie, WA 6433
[4]St Ives Gold Mining Company (Pty) Limited, PO Box 359, Kambalda West, WA 6444
[5]Mineral Mapping Pty Ltd, 24 Webb St, Rossmoyne, WA 6148
John.Walshe@csiro.au

Introduction

From a conceptual perspective, multi-fluid systems and contrasting fluid chemistry should be considered the norm for mineral systems. The rate of mineralisation is dependent on the magnitude of the physicochemical gradients within systems, and mixing of chemically contrasting fluids is a highly effective mechanism of sustaining gradients. Phillips (1990) defines the rate of mineralisation (R) for steady state conditions as:

R = Fluid velocity • Σ (Change of solubility with P,T, concentration × Gradient of P,T, conc)

According to this description of the rate of mineralisation, three factors are important:

1. Velocity of fluids
2. The solubility sensitivity of elements in the fluids as a function of physicochemical parameters (P,T, redox, pH, salinity, etc)
3. The spatial gradients of these physicochemical parameters.

An implication of models of mineralisation that utilise fluid mixing to sustain physicochemical gradients is that pathways of the different fluids must be apparent in the geology. There should be quite specific relationships between types of structures in the architecture, types of alteration and geodynamic history. If this were not the case, then the chemical potential of fluids would be degraded along the flow paths, and the capacity of the system to create chemical contrasts at specific sites would be lost. It should be possible to map the pathways at scales larger than the deposit and utilise the knowledge of these pathways in exploration. Conversely, if there is degradation of chemical potential of the end-member fluids by fluid-fluid and fluid-rock interactions, then it ought to be possible to recognise and map the alteration products of these events. Arguably, if the processes of ore formation are inherently inefficient processes, then the 'degraded' alteration patterns will be the common footprints in the system that need to be 'navigated' to locate the productive pathways and sites of fluid mixing. The example of black smokers on the modern seafloor suffices to illustrate how inefficient nature can be at fixing metals on some physicochemical gradient.

Mapping fluids pathways: St Ives Goldfields

Three distinct end-members fluids are required to explain the fluid inclusion, geochemical, mineralogical and isotopic characteristics of the gold systems in the Eastern Goldfields, Yilgarn Craton (Figure 1). Fluid 1 is considered a volatile-poor, aqueous crustal fluid, most likely derived from the late basins. Fluids 2 and 3 are considered anhydrous, volatile-rich, 'deep-Earth' fluids. Pathways, and domains of mixing and interaction between these end-member fluids, may be mapped using a combination of mineralogical, isotopic and architectural constraints. The stable isotopes are particularly sensitive indicators. The stable isotopes of C and S are sensitive to redox changes, that is, changes in the ratios of $H_2/CH_4/CO_2/SO_2$ or sulfate in the fluids and the $^{18}O/^{16}O$ ratio is sensitive to variations in H_2O/CO_2. Figures 2 to 4 illustrate the mapping of reduced, oxidised and anhydrous fluid pathways and definition of chemical gradients in the Victory- Defiance (Leviathan Complex), St Ives Goldfield.

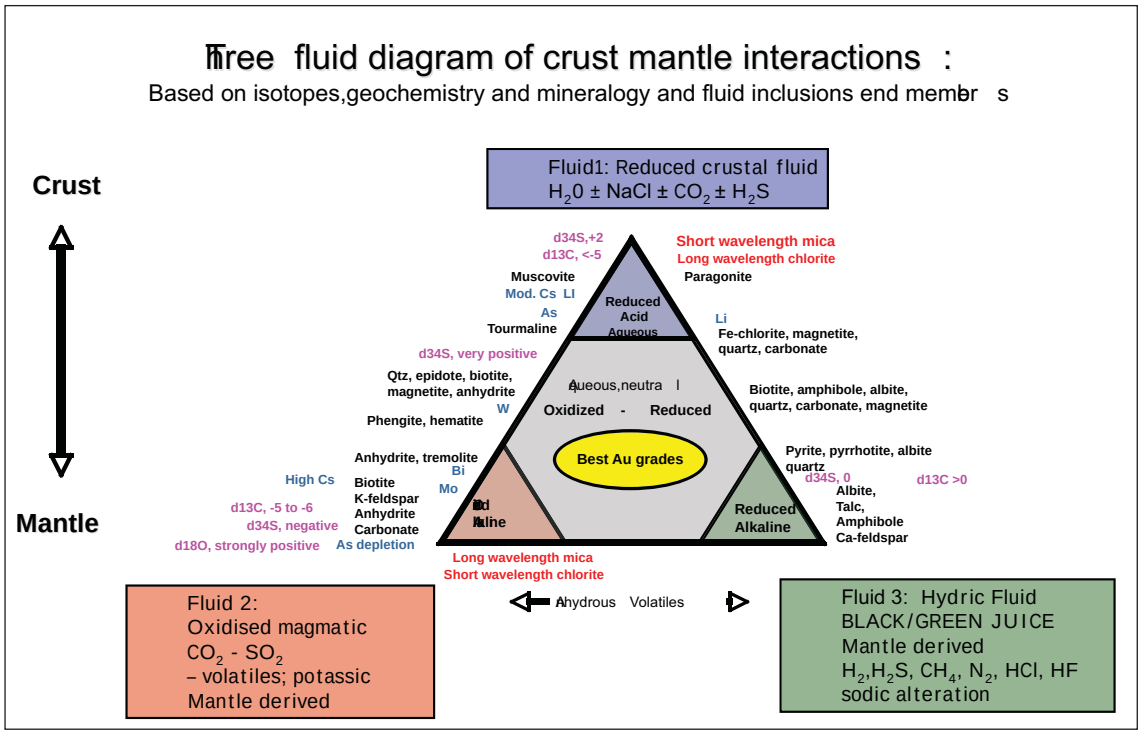

Figure 1. Schematic illustration of relationship of alteration minerals, isotopes and geochemistry to end-member fluids of gold systems of the Eastern Goldfields, Yilgarn Craton. Fluid 1 is considered to be an ambient crustal fluid, which is aqueous with low concentrations of salt and volatiles. Fluids 2 and 3 and are considered anhydrous, volatile-rich 'deep-Earth' fluids

The salient interpretations of the stable isotope data (see summary values in Figure 4) are:

1. The negative departures of $\delta^{13}C$ carbonate and $\delta^{34}S$ pyrite from the dominant reservoir values for $\delta^{13}C$ CO_2 (~ -5 to -6 ‰) and $\delta^{34}S$ sulphur (~ 0 ‰) are taken to reflect dominance of oxidised species such as SO_2 or sulfate over reduced species such as H_2/CH_4.
2. The positive departure of $\delta^{34}S$ pyrite from the dominant reservoir of $\delta^{34}S$ sulphur is taken to reflect dominance of reduced species, either H_2 or CH_4 over oxidised sulfur species.
3. The dominance of H_2 in the fluids is tracked by positive departures of $\delta^{13}C$ carbonate from the dominant reservoir of $\delta^{13}C$ CO_2, reflecting the reduction of oxidised carbon species e.g. $CO_2 + 4H_2 = CH_4 + 2H_2O$.

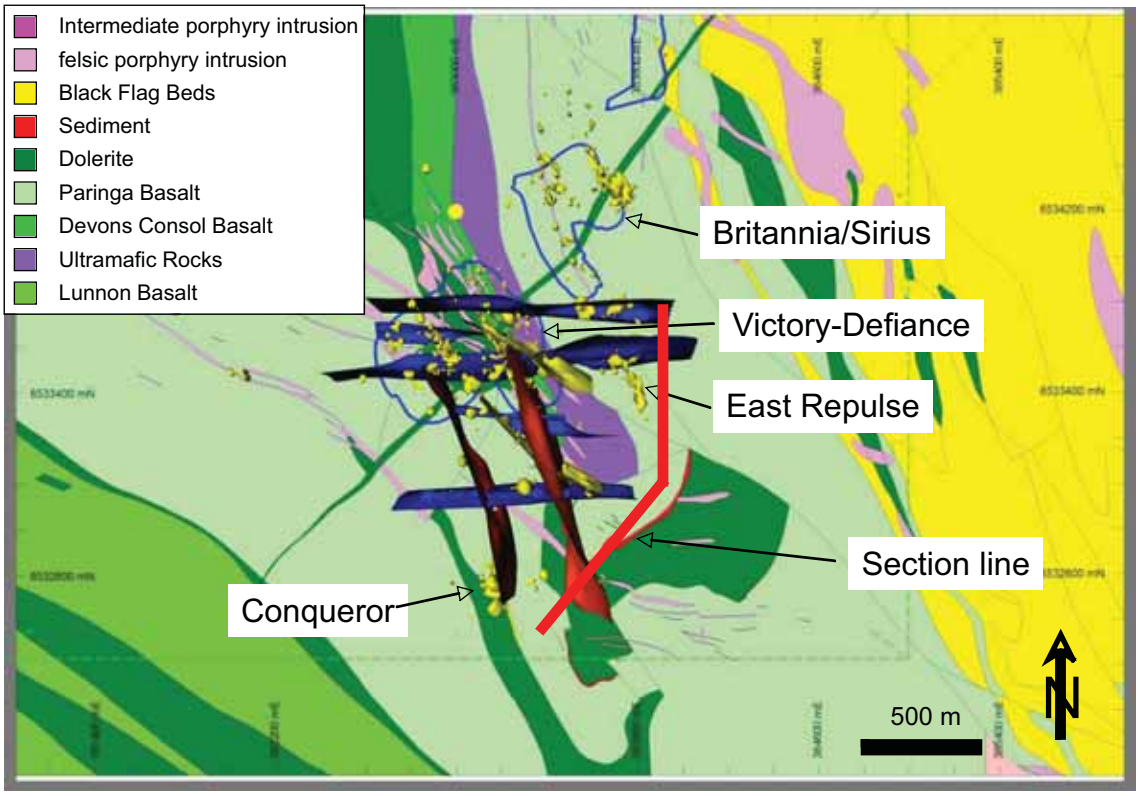

Figure 2. Map of the Victory-Defiance (Leviathan) complex showing the geology, distribution of open pits, and the location of 3 g/t gold ore shells, as modeled in Leapfrog. Location of interpreted east-west to east-southeast – west-northwest trending structures is shown in the blue surfaces. Section line for Figures 3 and 4 is indicated.

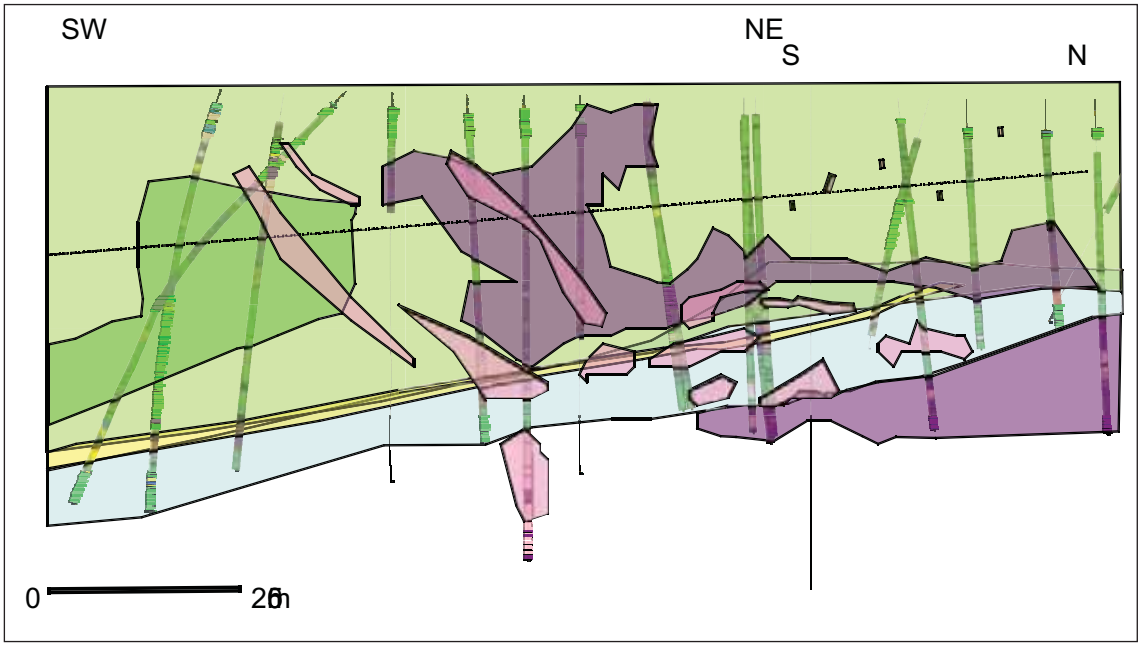

Figure 3. Geology along section line shown in Figure 2, with selected drillholes. Geological legend as for Figure 3 (expect the lower basalt, Devons Consol Basalt, shown in blue). Variation of stable isotopes of $\delta^{34}S$ pyrite, $\delta^{13}C$ carbonate and $\delta^{18}O$ carbonate and inferred alteration domains on this section are summarised on Figure 5.

4. The positive departures of $\delta^{18}O$ carbonate from dominant $\delta^{18}O$ value for the aqueous domain (see Figure 4) map anhydrous domains with CO_2 >> H_2O.

The mapped pathways, shown in Figure 4, are: -

- Up-flow zones of anhydrous oxidised fluids (Fluid 2)
- Lateral flow zones of oxidised hydrous fluids, resulting from mixing of Fluid 1 and Fluid 2.
- Upflow and lateral flow zones of reduced fluid that is a mixture of Fluid 1 and Fluid 3.

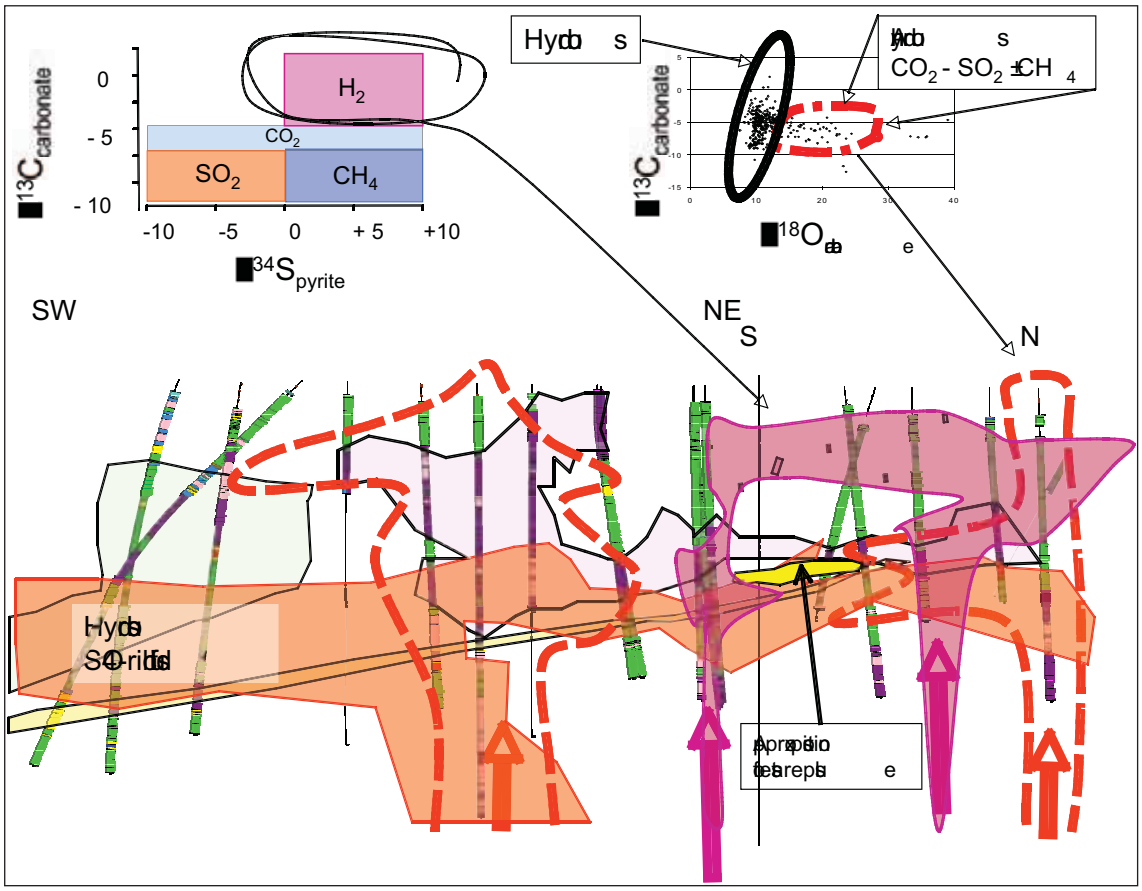

Figure 4. Geological section with interpreted domains of oxidised, reduced and anhydrous fluids, as mapped by $\delta^{34}S$ pyrite and $\delta^{13}C$ and $\delta^{18}O$ carbonate (lower figure). Key to isotopic interpretation shown in upper figures (as discussed in text). $\delta^{18}O$ carbonate > 13 ‰ is taken to indicate anhydrous CO_2 - SO_2 ± CH_4 fluids. $\delta^{13}C$ carbonate > -4 and $\delta^{34}S$ pyrite > 0 ‰ is taken to indicate reduced hydrous domains with H_2 dominant in fluid. $\delta^{13}C$ carbonate < -6 and $\delta^{34}S$ pyrite < 0 ‰ taken to indicate oxidised hydrous domains with aqueous sulfate dominant in fluid.

Gradient, depositional processes and targeting

Significant gradients in redox, pH, water activity, sulfur activity and salinity gold were developed in the gold systems of the Eastern Goldfields (Walshe et al., 2006). Gold was apparently transported by either Fluid 3 and/or Fluid 2 under anhydrous conditions and decoupled from transport and deposition of most other elements. Gold deposition occurred over a wide range of redox conditions (Figure 5), mostly in neutral to alkaline pH conditions (phengite rather than muscovite, i.e. long versus short SWIR wavelength). The transition from hydrous to anhydrous environment appears to be important. Gold depositional reactions leading to the formation of high-grade Au deposits is taken to be highly specific and involve little water,

hence the lack of alteration in the immediate vicinity of high grade gold zones, and the overall lack of correlation with any specific mineral or mineral assemblage. Gold transferred to the aqueous - acidic fluids by mixing of 'deep-Earth' fluids with ambient aqueous fluids drove district-scale acidic alteration and dispersion of Au. These fluids mobilised many rock-forming elements, including iron, and generated widespread alteration. Mapping gradients developed between Fluid 2 and Fluid 3, with limited input of Fluid 1, appears to provide the offer the best opportunities for targeting using gradient mapping.

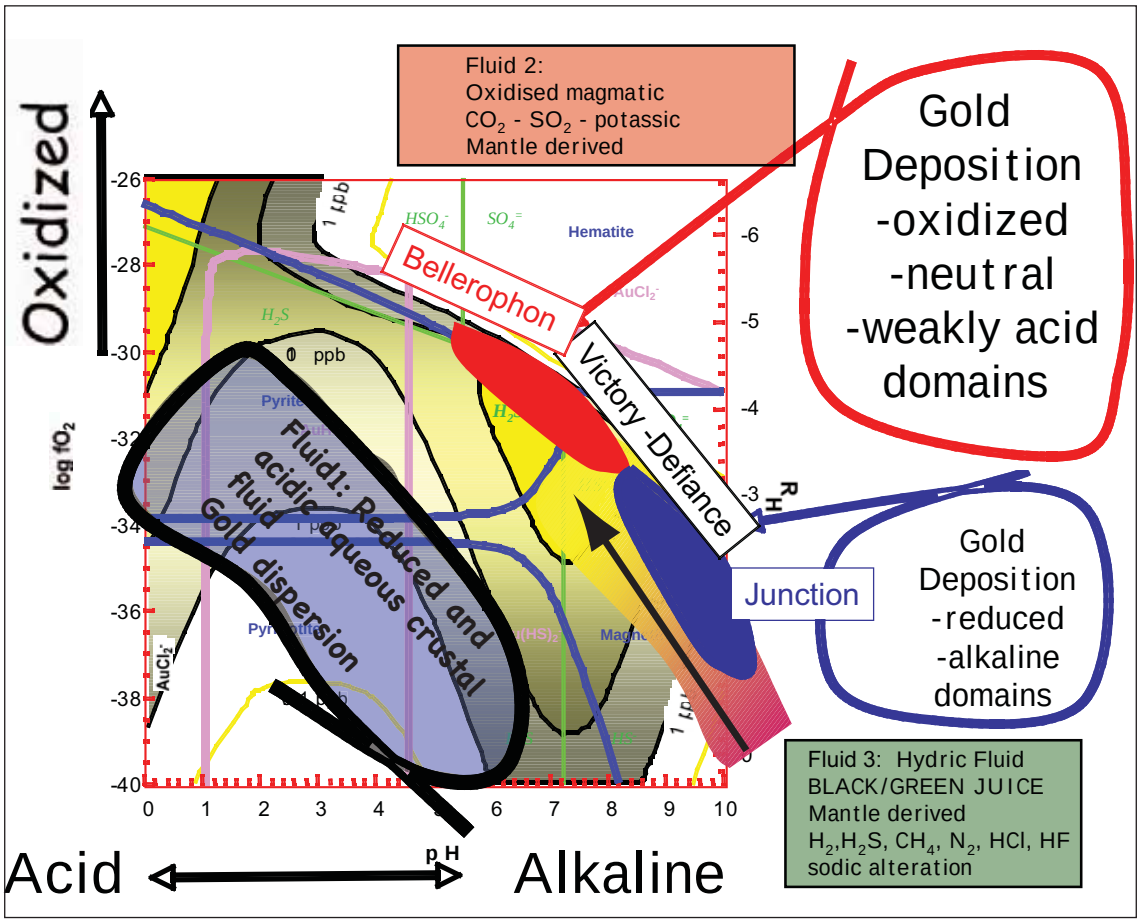

Figure 5. Illustration of Au transport and deposition conditions. It is assumed that gold complexed in Fluid 3 (hydric fluid) is transferred to aqueous bisulphide complex at neutral to alkaline conditions and moderate oxidation states. Gold in reduced and acidic fluids is dispersed.

References

Phillips, O.M., 1990. Flow controlled reactions in rock fabrics. Journal of Fluid Mechanics, 212, 263-278.

Walshe, J.L., Neumayr, P., Petersen, K.J., Young, C. & Roache, A., 2006. Scale-integrated, architectural and geodynamic controls on alteration and geochemistry of gold systems in the Eastern Goldfields Province, Yilgarn Craton. MERIWA Project 358, Final Report, 287pp.

Architecture: Fluid flow modelling at Fosterville, Victoria

CHRISTOPHER J.L. WILSON, LAWRENCE D. LEADER AND JAMIE A. ROBINSON

*pmd***CRC*, School of Earth Sciences, The University of Melbourne, VIC 3010
cjlw@unimelb.edu.au

Introduction

Gold mineralisation at Fosterville is hosted in a Ordovician turbidite succession and is characterised by fine-grained microscopic gold embedded in a matrix of disseminated pyrite and arsenopyrite that is located in either faults or bedded units. The host rocks are dominated by tight, chevron-shaped folds, with weak cleavage development that trend 335°-340°. These folds exhibit shallow plunge reversals and have average limb dips of ~70°, with increased gold grades only occurring where the folds are intersected by faults.

In sandstone units, adjacent to faults and within fold hinges, there is extensive quartz-carbonate veining, suggesting that these units have been subjected to numerous fluid overpressure and tensile failure events. Mudstone units are also characterised by quartz-carbonate veining, however, the extent of the veining is limited to thin veins that are parallel to the slaty cleavage, with little or no quartz-carbonate veining oblique to the cleavage. This implies that the mudstone units have not been subject to tensile failure and have only undergone a small amount of dilation along the cleavage planes.

Low-displacement faults (e.g., Phoenix Fault), clustered as west-dipping splays off the higher displacement, regional-scale Fosterville Fault, also control the gold mineralisation. Anomalous gold grades are found at localities in which the hangingwall bedding is oblique to the fault and the footwall bedding is parallel to the fault. The extent to which this geometric relationship controls deformation, fluid flow and hence mineralization has been investigated by a series of FLAC 2D and FLAC 3D (Fast Lagrangian Analysis of Continua) numerical models, in which the angle between bedding in the footwall and hangingwall of a fault is varied to determine a geometry for optimum fluid flow.

Workflow

The workflow developed to understand these primary structural controls on mineralisation was designed in light of the following considerations:

(1) Evaluation of the geometries of the folds and the west-dipping faults associated with mineralisation and how they relate to two sets of slickenlines (Figure 1). The first set of fault-related slickenlines is subvertical and plunge steeply to the west. This set of slickenlines is approximately perpendicular to the bedding-cleavage intersection lineations and are also found on bedding interfaces, implying that they are a result of flexural slip during folding. The second set of slickenlines plunge at a shallower angle towards the northwest. The presence of sulphides on these slickensides suggests that these slickensides are indicative of the transport direction associated with mineralisation. The transport direction is northwest over southeast with a component of sinistral movement. This is also consistent with sinistral, transpressive kinematics suggested by Wang and White (1993) as being related to mineralisation in the Fosterville and Heathcote areas.

(2) A 3D model of the Fosterville deposit, constructed using gOcad™, was based upon surfaces provided by Northgate (Figure 1), to form the geometric basis for the construction of three-dimensional deformation-fluid flow models of the ore body.

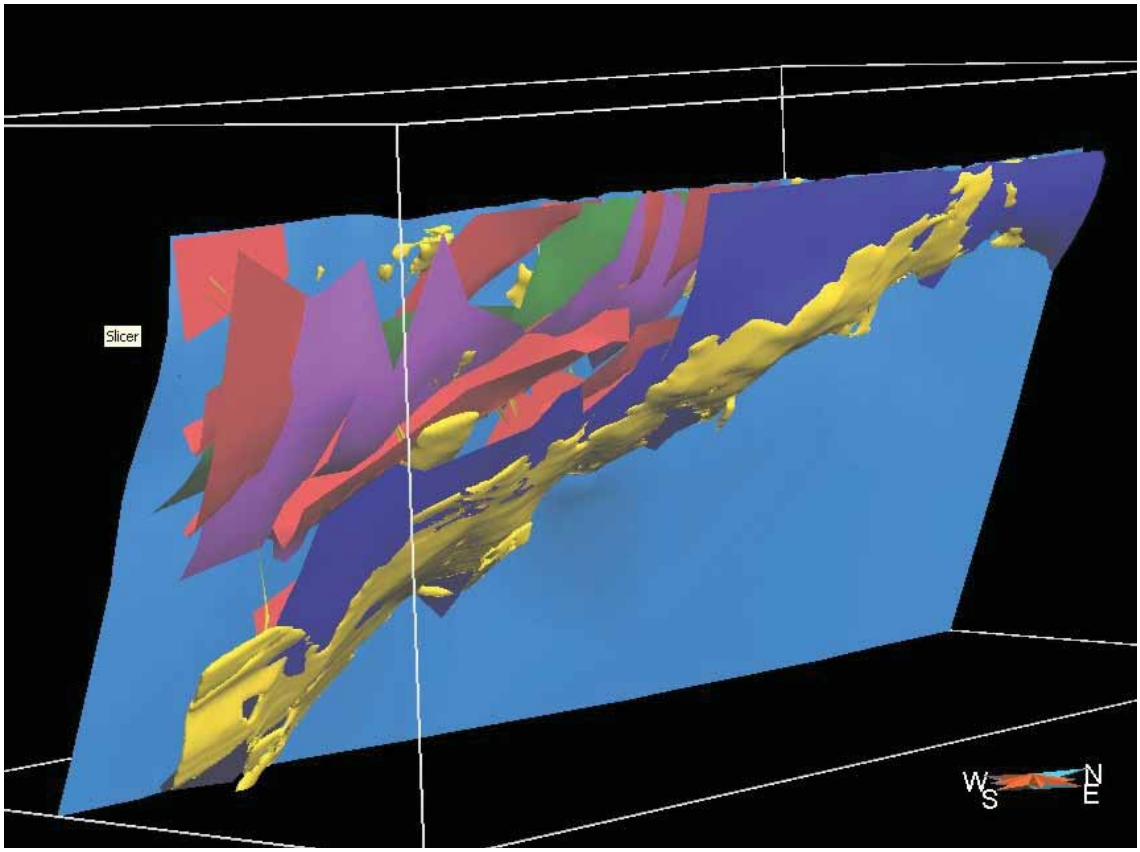

Figure 1. 3D model of the Fosterville deposit viewed from the east. Bedding is shown in red, 3.5 g/t grade shells in yellow and the Fosterville (light blue), Hawk (green), Kite (purple) and Phoenix (dark blue) faults. Striations on the surface of the Phoenix fault shown on the stereographic net indicate west-over-east and northwest-over-southeast directed transport with the northwest-over-southeast transport occurring at high-angles to the plunge of the fault-bedding intersection. The bedding-fault intersection is plotted on the stereonet (So). Note the obliquity between the inferred northwest-over-southeast transport direction and the bedding-fault intersection.

(3) A palaeostress analysis of fault slickenline striations using the software SLICK.BAS (Ramsay & Lisle, 2000) has yielded a maximum principal stress (σ_1) of 26° to 314° that is related to an east-west compression. Some conjugate northwest and southwest-dipping faults and extension vein arrays, however, can be related to a north-south σ_1 direction.

(4) 3D deposit scale models were constructed to investigate the importance of the domal culmination in controlling the mineralisation. The models extend over a distance of 9 km by approximately 2.8 km in height (Figure 2). The geometries used in the models are simplified, such that splay faults off the Fosterville Fault are represented by a single fault (Phoenix), whereas bedding is also simplified to remove fold hinges while maintaining bedding parallel-parallel and oblique-parallel relationships with the adjacent Fosterville and Phoenix Faults.

(5) 2D models were then constructed in the plane of the interpreted maximum and minimum principal stresses (σ_1 and σ_3), where the angle between the fault and bedding in the hangingwall

and footwall of the fault is varied, to determine what geometry is ideal for optimum fluid flow into the adjacent psammitic rocks. The bedding-fault angle is measured from the bedding through to the fault in a clockwise direction with bedding units rotated by 10° from one model to the next, so that bedding-fault angles of 50° through to 150° are considered.

(6) The mechanical and physical properties were modified from Schaubs and Zhao (2002), after calibrating them against known structural behaviour of the rocks within the Fosterville mineralised system. The models are given an overburden of 4.2 km, based on constraints placed by the regional metamorphic and intrusive history (Offler et al., 1998; Bierlein et al., 2001). Initial compressional velocities are applied to the sides of the models, which were allowed to deform to a value of 1% shortening. The fluid conditions were set to near lithostatic conditions (~80%) at the initiation of shortening.

3D modelling

The results of the three-dimensional numerical modelling suggest a strong relationship between the plunge of the faults-bedding intersections and mineralisation. Current targeting of gold in the Fosterville deposit focuses on a relationship between regions of the faults that cross-cut the stratigraphy at high angles, whereas regions in which the faults occur parallel to bedding are know to be associated with relatively poor gold content and only localised distribution. In the three-dimensional numerical deformation-fluid flow model, highest dilation occurs where the bedding-fault intersection plunges shallowly to the south (for the west-dipping faults), which shows strong correlation to the distribution of gold at Fosterville (Figure 3). The plunge of the intersection occurs sub-perpendicular to an episode of reverse-oblique, northwest over southeast movement indicated by striations on fault surfaces. In this case, the relationship between fault transport direction and the plunge of bedding-fault intersection may provide an important control on dilation and fluid flow, and also provide further targets for mineralisation on faults formed during northwest-southeast compression. Furthermore, these results indicate that northward plunging intersections are not good targets for disseminated mineralisation within wall rocks.

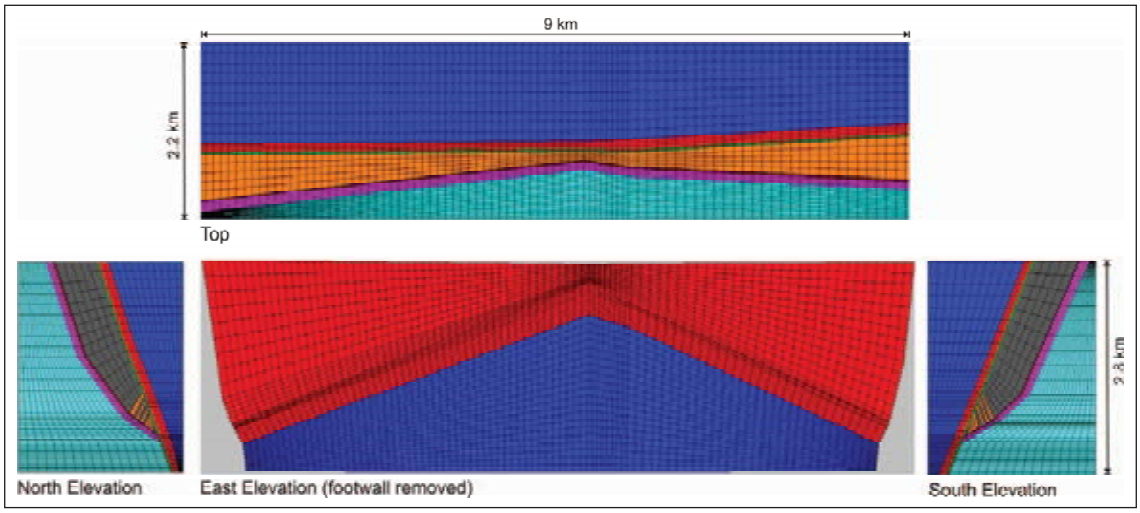

Figure 2. Model geometry of the principal surfaces at Fosterville in FLAC 3D.

2D modelling

The geometry of these models consisted of a west-dipping fault with alternating layers of mudstone and sandstone adjacent to the fault. The angle between the fault and layers of mudstone and sandstone is changed from one model to the next so that the series of models consider bedding-fault angles that

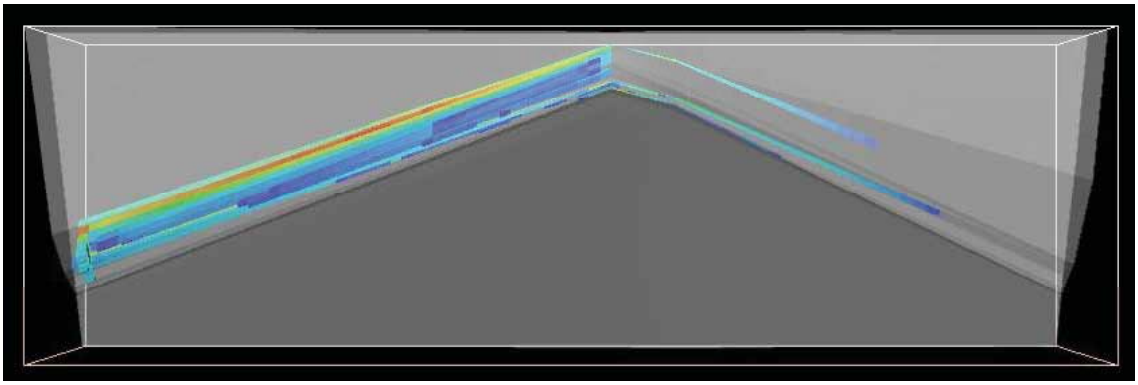

Figure 3. Volume strain indicating dilation in the psammitic units between faults at 1% shortening (looking west). The dilation ends at the plunge reversal as does the mineralisation within the grade shell model in Figure 1.

range from 50° to 150°. Volumetric strain plots and fluid flow plots (Figure 4), for the regions of the models in which there are variations in the orientation of the hangingwall bedding at fault angles of 70°, 65° and 60°, show that the greatest amounts of dilation occur along the fault and within the sandstone units at low bedding-fault angles and at the unit boundaries at high bedding-fault angles. Fluid flow plots show that the extent of fluid flow within the metasedimentary wall-rocks decreases as the bedding-fault angle is increased from 50° to 70°, and then increases as the bedding-fault angle is increased to 150°.

The magnitude of the fluid flow rate in the sandstone units of the hangingwall can also be recorded as flow rate versus bedding-fault angle plots (Figure 5). These plots show that the magnitude of fluid flow varies with bedding-fault angles. The plots also show that at low bedding-fault angles, a low magnitude of fluid flow within the stratigraphically lower sandstone unit is mirrored by a higher magnitude of fluid flow in the stratigraphically higher unit. Conversely, at high bedding-fault angles a high magnitude of fluid flow in the stratigraphically lower sandstone is mirrored by a lower magnitude of fluid flow in the stratigraphically higher unit.

Flow rate versus bedding-fault angle plots for changes of the footwall-bedding-fault angle show a similar relationship between fluid flow and bedding-fault angles (Figure 6). Generally, the fluid flow rate is higher at low hangingwall-bedding-fault angles, and decreases to a minimum at a bedding-fault angle of 80°. Fluid flow then increases as the bedding-fault angle is increased to 150°.

Stress field variations and their influence on dilation

The 2D models have been further modified to consider variations in the magnitude of the maximum principal stress direction (σ_1) relative to the intermediate principal stress (σ_2) and how this affects the distribution of dilation within the FLAC 3D models. As the strike-slip to contraction ratio increases from 0 to 1, the value of σ_2 increases from being significantly less than σ_1 to being equal to σ_1. Ratios of σ_2:σ_1 greater than 1 imply that σ_2 is greater than σ_1, and therefore the maximum principal stress direction changes from east-west to north-south. Through the use of a number of iterative models, it can also be shown that the distribution of dilation in beds with a bedding-fault angle of 50° can be observed to increase in the sandstones as the σ_2:σ_1 increases from 0.5 to 1.0 and then decreases as the σ_2:σ_1 ratio is increased from 2.0 to 3.0 (Figure 7). Similarly, for a bedding-fault angle of 120°, dilation is restricted to the faults and sandstone units, however, the extent and magnitude of dilation within the sandstone units is considerably less. The results are consistent with the results of the 2D models and field observations.

Conclusion

The implications of these models are that the geometry of bedding and faults in combination with applied stress fields and resultant hangingwall transport directions influence fluid flow and the potential location

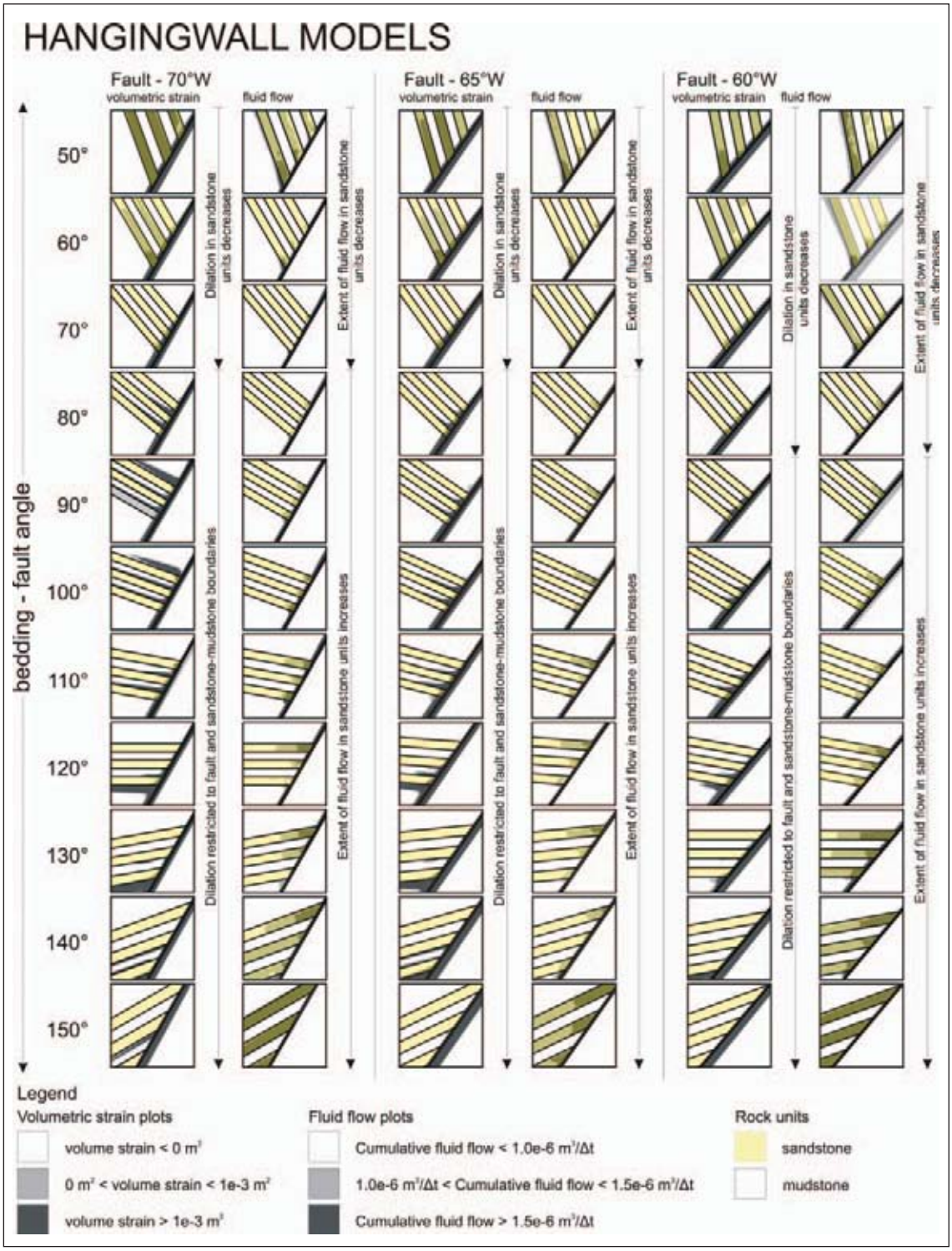

Figure 4. Volumetric strain (dilation) plots and cumulative fluid flow plots in the hangingwall of three models that represent faults dipping at 70°, 65° and 60° west. All results are shown at 1% shortening.

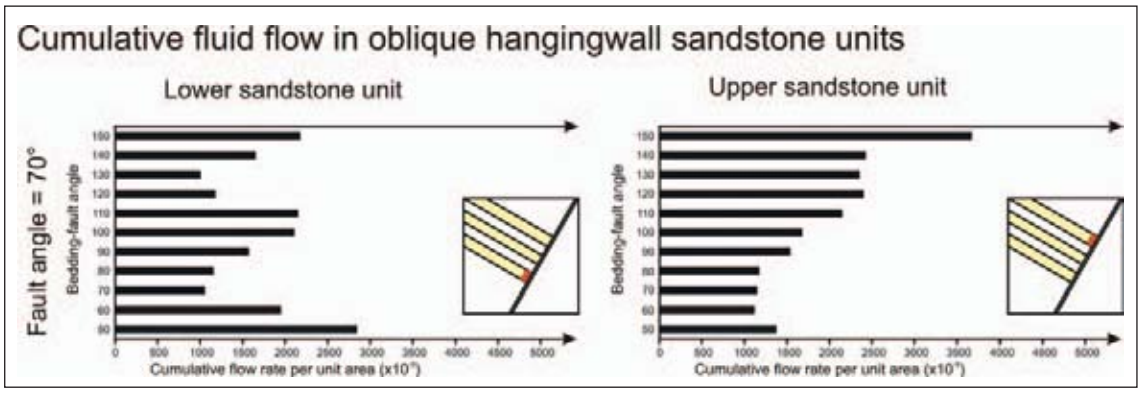

Figure 5. Bar graphs of cumulative fluid flow within the lower and upper oblique hangingwall sandstone units adjacent to a 70° west-dipping fault. The red regions of the inserts illustrate the parts of the sandstone from which the cumulative fluid flows have been averaged and graphed. In the lower unit a maximum occurs at a bedding-fault angle of 50°, although there is significant fluid flow at bedding-fault angles of 100°, and 110°. In the upper sandstone, the maximum is at 150° and the minimum is at 60°.

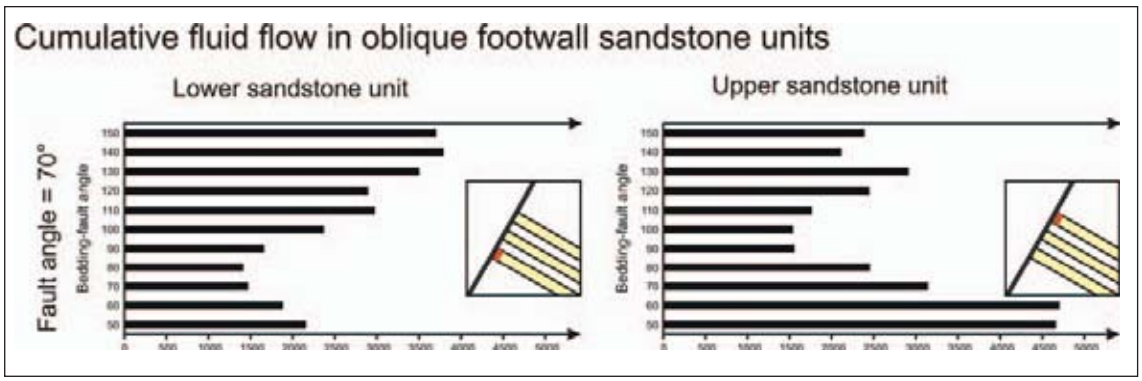

Figure 6. Bar graphs of cumulative fluid flow within the lower and upper oblique footwall sandstone units adjacent to a 70° west-dipping fault. The red regions of the inserts illustrate the parts of the sandstone from which the cumulative fluid flows have been averaged and graphed. In the lower unit, a maximum occurs at a bedding-fault angle of 140° and 150°, and in the upper sandstone the maximum is at 50° and 60°.

of mineralisation. Understanding the optimum geometric conditions producing dilation in potential host rocks adjacent to faults, and ranking fault bedding relationships based upon their potential to produce dilation may be a key tool for exploration in the Fosterville area. The results presented here correlate well with field data, which shows that significant gold grades occur at bedding-fault angles between 40° and 50°. Increased dilation, as influenced by these geometric relationships, would have facilitated the influx of gold-bearing fluids, which in combination with geochemical factors, have led to significant amounts of localised gold mineralisation.

Acknowledgements

The authors would like to thank Northgate Minerals Corporation for financial support and access to the open pits and underground workings at Fosterville. Neil Norris, Chris Reed, Simon Hitchman and the geological team at the Fosterville Gold Mine are thanked for their on-site assistance and advice. Peter Schaubs from the computational modelling group of CSIRO Exploration and Mining is thanked for his help in the early stages of facilitating this modelling project.

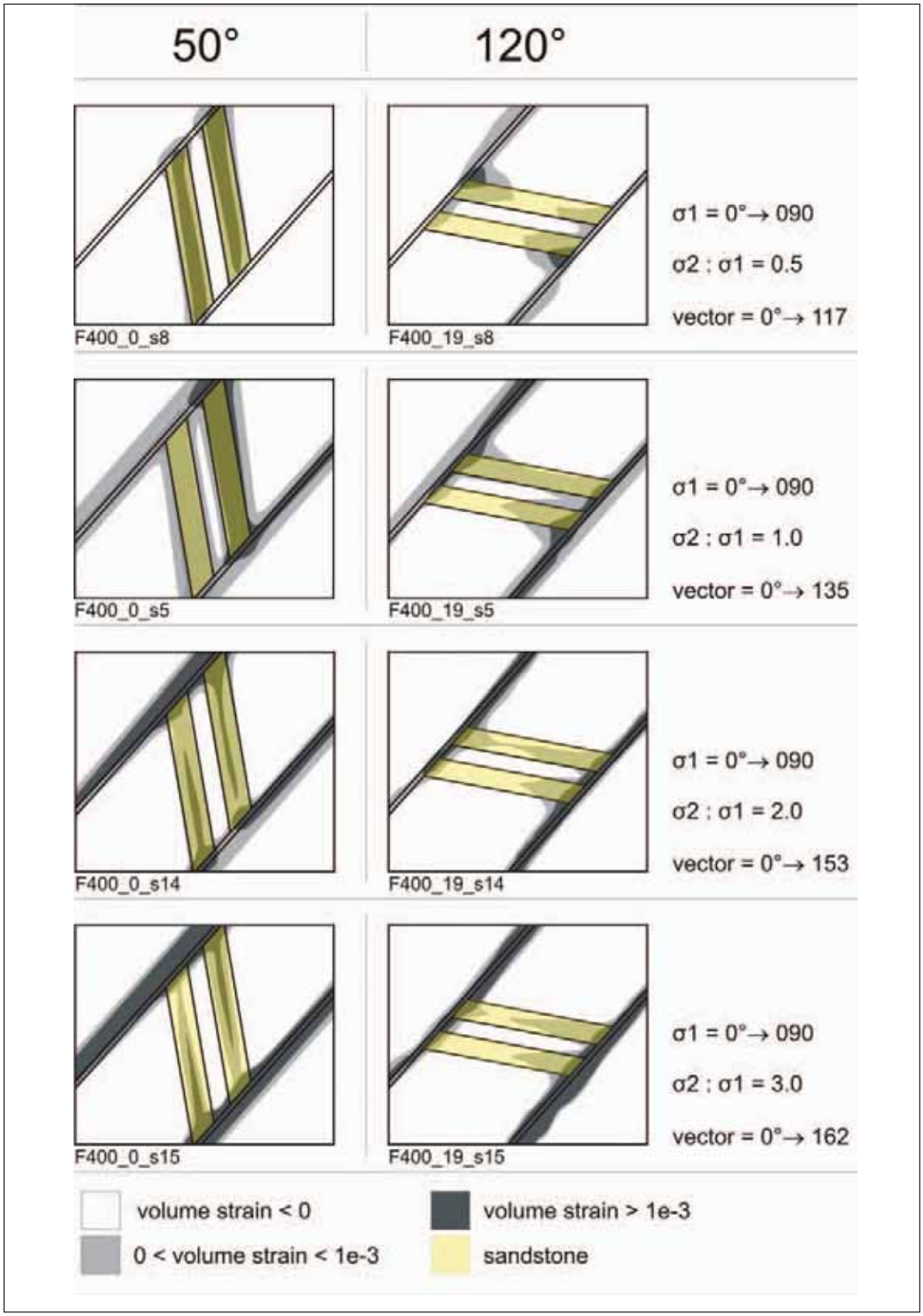

Figure 7. Distribution of dilation at 1% shortening with increasing values of σ_2:σ_1 that produces a resultant vector which is within the range of the observed slickenline orientations.

References

Bierlein, F.P., Arne, D.C., Foster, D.A. & Reynolds, P., 2001. A geochronological framework for orogenic gold in central Victoria, Australia. Mineralium Deposita, 36, 741-767.

Offler, R., MCKnight, S. & Morand, V.J., 1998. Tectonothermal history of the western Lachlan Fold Belt, Australia: insights from white mica studies. Journal of Metamorphic Geology, 16, 531-540.

Ramsay, J.G. & Lisle, R.J., 2000. The techniques of Modern Structural Geology, Volume 3: Applications of continuum mechanics in structural geology. Academic Press. London, 701-1061pp.

Schaubs, P.M. & Zhao, C., 2002. Numerical models of gold deposit formation in the Bendigo-Ballarat Zone, Victoria, Australia. Australian Journal of Earth Sciences, ,49, 1077-1096.

Wang, G.M. & White, S.H., 1993. Gold mineralization in shear zones within a turbidite terrane, examples from central Victoria, S.E. Australia; structural setting and controls on mineral deposits. Ore Geology Reviews, 8, 163-188.

Understanding regional structural controls on mineralisation at the Century deposit: a numerical modelling approach

YANHUA ZHANG[1], PAUL A ROBERTS[1], BARRY MURPHY[2], ANGELA LORRIGAN[3] AND RODNEY ANDERSON[3]

[1]*pmd***CRC*, CSIRO Exploration and Mining, Bentley, PO Box 1130, Bentley, WA 6102
[2]*pmd***CRC*, School of Earth Sciences, University of Melbourne, VIC 3010
[3] Zinifex Ltd, Level 29, Freshwater Place, 2 Southbank Boulevard, Southbank, VIC 3006
Yanhua.Zhang@csiro.au

Introduction

The Century zinc deposit, a world-class, sediment-hosted Zn deposit containing approximately 167 Mt of ore (in situ resource) grading 8.2% Zn, 1.2% Pb and 33 ppm Ag (Polito et al., 2006), is located on the Lawn Hill Platform of Northwestern Queensland, Australia. The Lawn Hill Platform, together with neighbouring areas in northern Australia, is the world's largest zinc province (Large et al., 2002), and there still exists huge potential for discovery of more world-class, Century-type deposits. Therefore, an improved understanding of the key controls on the formation of the Century deposit will be beneficial to future mineral exploration campaigns in the region.

A geological description of the Century deposit can be found in Broadbent et al. (1998). The origin of the sediment-hosted Zn-Pb-Ag deposits in the Isa Superbasin is a subject of ongoing debate (see Williams, 1998; Betts & Lister, 2002). Several studies (e.g., Feltrin, 2006; Feltrin et al., 2007) have advocated a syngenetic model for the formation of the Century deposit, although there is increasing evidence in support of an epigenetic replacement model. Broadbent et al. (1998) interpret mineralisation at Century as controlled by fluid flow during basin inversion on the basis of structural and mineral paragenesis data. This interpretation is supported by recent fluid inclusion and stable isotope data (Polito et al., 2006).

Numerical models have been used to explore the controls on fluid flow, and hence controls on mineralisation, in the Century district. Ord et al. (2002) used numerical models to explore fluid flow patterns associated with a highly simplified fault and stratigraphic architecture for Century (e.g. all the faults are vertical). Zhang et al. (2006) simulated tectonically-driven fluid flow in a 2D transect through the Lawn Hill Platform. The present numerical modelling study expands on these previous investigations by exploring deformation and fluid flow in a more realistic 3D architecture for the Century region. The models are used to examine possible mechanical controls on the locations of fluid focusing, and hence mineralisation, associated with tectonic inversion during the Isan Orogeny. The geometry of the model is based on a fault architecture derived from recent structural and geophysical work. We also consider the effects of stratigraphic units on fluid flow in the Century system. A key stratigraphic unit is the Widdallion Sandstone Member. Broadbent et al. (1998) interpreted clastic rocks of the Widdallion arkosic sandstone as forming a regional seal at the time of mineralisation. Because Century mineralisation

is hosted in a low permeability shale-siltstone unit (Pmh4), which is located immediately underneath the Widdallion Sandstone Member, a question arises as to how mineralising fluids can be focused into the low permeability Pmh4, and what role the Widdallion unit plays in this process. It is also interesting to consider how the stratigraphic controls are related to fault structures in the system.

The specific aims of this study are:

- How did the faults control fluid flow patterns in the Century District?
- What was the process that led to permeability creation and fluid focusing in the initially low permeability shale-siltstone rocks that host the Century ore bodies?
- What were the stratigraphic controls on these processes?

Model architecture

The model consists of a block of 50 km (northwest-southeast) x 85 km (northeast-southwest) x 25 km (depth), containing two northwest-southwest striking, major deep cutting faults, the Riversleigh Lineament (RL) and Termite Range Fault (TRF), and five cross faults (Figure 1). These fault structures are simplified interpretations of recent structural and geophysical interpretations. A simplified stratigraphic system is considered, including (from top to bottom) a cover unit, the Widdallion Sandstone Member, the seal-1 unit (H1-H4 successions of the Lawn Hill Formation and Riversleigh Formation), including one or two thin weaker layers embedded within it, Shady Bore Quartzite (aquifer), the seal-2 unit (Lady Loretta Formation and Lower McNamara Group), Fiery Creek Volcanics (FCV, another inferred aquifer), and the basement. The mineralised host rocks (Pmh4) lie at the top of the seal-1 unit, immediately below the Widdallion unit. The Century deposit is located at this level, at the intersection of the TRF with the Little Archie Fault. Detailed geometrical features are illustrated in Figure 1 and properties of the stratigraphic units and faults are given in Table 1. The Widdallion unit is simulated as a low permeability unit, as suggested by Broadbent et al. (1998), although the higher permeability case is also tested.

It is worth noting that the TRF and RL form a 'Y-front' architecture, similar to that proposed for major faults in the Yilgarn Craton (Drummond et al., 2000). Two main scenarios are simulated:

- Scenario 1 (Figure 1a): the RL is buried below the Widdallion unit and the TRF is exposed at the surface. This scenario is based on the present-day surface geology and interpretation from potential field data;
- Scenario 2 (Figure 1b): the RL is buried deeper in the succession and the TRF is modelled as a buried fault below the Widdallion unit. This reflects a possibility that the TRF ceased to have syn-sedimentary movement prior to the D1 event (northwest-southeast shortening) and that this cessation of movement may have coincided with incipient inversion and change of sedimentary provenance (Peter Southgate, pers. comm.) at the onset of the Widdallion sedimentation. The current TRF outcrop would therefore be the result of the D2 inversion (north-south shortening). Given that the RL does not outcrop, its upper tip may have been significantly deeper than the TRF prior to the D1 event; otherwise it should have been inverted in a manner similar to the TRF.

Cross faults in both scenarios are assumed to be buried below the Widdallion unit. We have also explored subsets of these scenarios with the TRF and RL being vertical (which we describe as the 'H-front' scenarios).

Model methodology

FLAC3D version 3.0 (Itasca Consulting Group, 2005) was used for the present modelling. The code is capable of simulating interactions between deformation and fluid flow in porous media. In a FLAC3D model, rocks are simulated as Mohr-Coulomb isotropic elastic-plastic materials. The constitutive parameters include shear modulus, bulk modulus, cohesion, tensile strength, friction angle and dilation

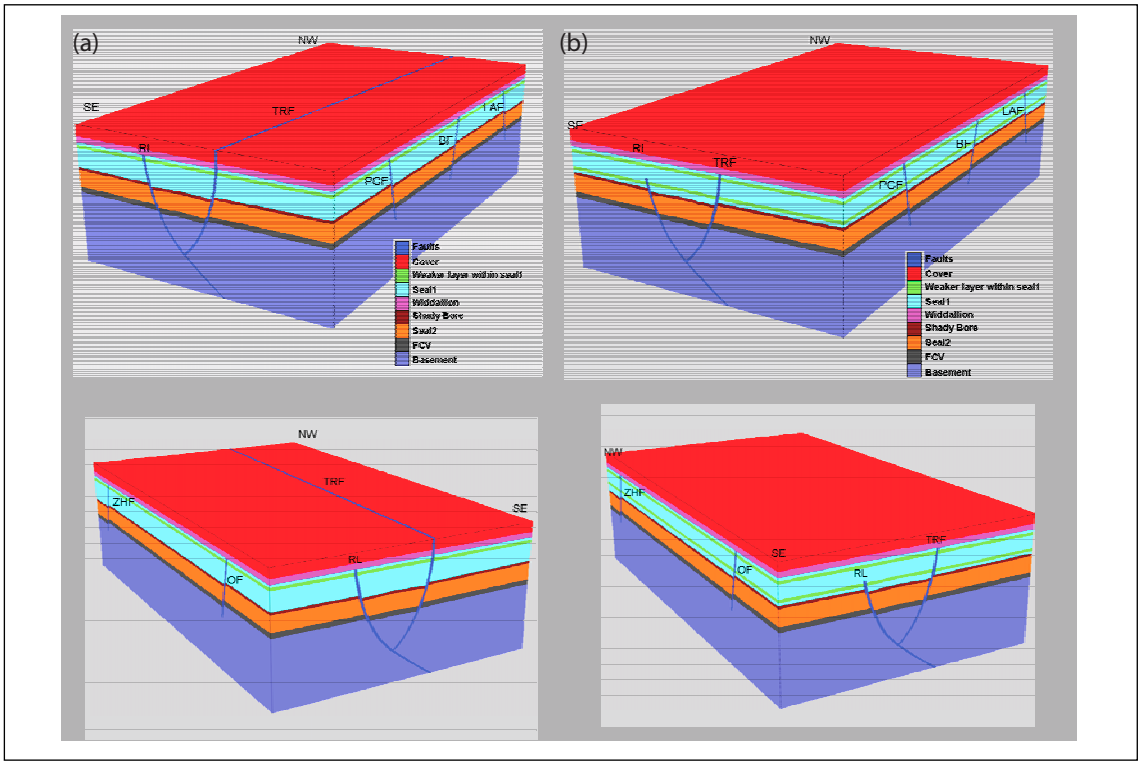

Figure 1. 'Y-front' model geometries. a) Scenario with the RL buried below the Widdallion Sandstone Member and the TRF exposed to surface. b) Scenario with the RL buried deeper in the succession and the TRF buried immediately below Widdallion Sandstone Member. TRF – Termite Range Fault; RL – Riversleigh Lineament; PCF – Police Creek Fault; BF – Barramundi Fault; LAF – Little Archie Fault; OF – O'Shanessy Fault; ZHF – Zinc Hills Fault. The Pmh4 horizon lies at the top of the seal-1 unit. The green layers below the upper ends of the RL and TRF are weaker layers with the lowest tensile strength (see Table 1).

angle. Under loading, such materials deform elastically up to a yield point (i.e., before the maximum shear stress reaches a threshold magnitude), after which it deforms in a plastic manner. Fluid flow in the models is governed by Darcy's law for an isotropic porous medium. As such, fluid flow velocities are primarily a function of gradients in pore fluid pressure, and variations in permeability. Fluid flow is coupled with mechanical deformation during the simulation (e.g., dilation results in decreasing fluid pressure and thus influences fluid flow). All the models are deformed to 15% bulk shortening. The initial fluid pore-pressure gradient is about 50% of the lithostatic gradient. Such initial pore-pressure gradient is fixed at the left and right sides (the sides subparallel to the Termite Range Fault) of the model, approximately down to the base of sediment succession (above the top of basement), approximately simulating the possible fluid supply from the lateral far-field regions of the basin.

Model results

Scenario 1 – exposed TRF and buried RL

The architecture of the scenario 1 model (the RL buried below the Widdallion unit and the TRF exposed at the surface) is deformed by northwest-southeast shortening (the D1 event which probably began as early as 1595 Ma). The results are presented in Figure 2. There is clear development of tensile failure, permeability enhancement, higher dilation, and fluid flow focusing and mixing around the top end of the buried RL at the Pmh4 level (top of the seal-1 unit). These effects are localised at the intersections of the RL with the Zinc Hill Fault and O'Shanessy Fault near the Pmh4 shale-siltstone seal package and

Table 1. Stratigraphic units and material properties of the models (see Fig. 1 for geometries)

Rock unit	Density ($kg.m^{-3}$)	Young's modulus (Pa)	Poisson ratio	Bulk modulus (Pa)	Shear modulus (Pa)	Cohesion (Pa)	Tensile strength (Pa)	Friction angle	Dilation angle	Permeability (m^2)	Porosity
Cover Unit (H6 or post Widdallion	2400	2e10	0.2	1.11e10	8.33e9	1.0e7	1e6	25	3	4e-15	0.2
Widdallion sandstone & siltstone	2450	3.5e10	0.25	2.33e10	1.4e10	2.0e7	2e6	30	3	2e-18	0.15
Seal 1 (H1-H4 of 0.05Lawn Hill Fm & Riversleigh FM)	2480	3e10	0.25	2.0e10	1.2e10	1.5e7	1e6	30	3	1e-18	
Weaker layers in Seal1 (with horizontal fabrics)	2440	2.2e10	0.25	1.47e10	8.8e9	1.2e7 (jcoh=6.0e6)	0.5e6	30	3	1e-18	0.05
Aquifer (Shady Bore Qtz)	2500	4e10	0.25	2.66e10	1.6e10	2.5e7	2.5e6	30	3	2E-15	0.1
Seal 2 (Lady Loretta & Lower McNamara)	2580	5e10	0.25	3.33e10	2.0e10	3.0e7	3.0e6	30	3	1e-18	0.05
Aquifer (FCV)	2900	6e10	0.25	4.0e10	2.4e10	4.0e7	4.0e6	30	3	2E-15	0.1
Basement	2650	7e10	0.25	4.66e10	2.8e10	5.0e7	5.0e6	30	1	1e-18	0.05
Faults	2400	1e10	0.15	4.8e9	4.25e9	8e6	0.8e6	25	3 (1 for basement level)	2E-14	0.1

Widdallion Sandstone Member contact. In contrast, there is little evidence of these effects near the TRF that is connected to the surface. The factors critical to such development are: 1) a buried RL leading to the accumulation of fluids and build-up of pore pressure; 2) the low permeability of the Widdallion unit (arkosic sandstone, sandwiched with shale and siltstone), which helped to trap fluids and maintain pore pressure at the level immediately below the Widdallion unit; 3) tensile failure leads to permeability enhancement and localised dilation; and 4) enhanced permeability and dilation attract fluids, resulting in fluid focusing and mixing. The results of this scenario are inconsistent with the location of the Century deposit at the intersection of the TRF with the Little Archie Fault.

Scenario 2 – buried TRF and deeper buried RL

The architecture of the scenario-2 model (the TRF buried below the Widdallion unit and the RL buried deeper in the succession) is also deformed under the D1 northeast-southwest shortening conditions. The results are summarised in Figure 3. The development of tensile failure, permeability enhancement, high dilation and fluid flow focusing/mixing is now localised around the intersections of the TRF with the cross faults (Little Archie, Police CK and Barramundi) at the Pmh4 level. Interestingly, the level near the upper end of the more deeply buried RL does not show any tensile failure, permeability enhancement and dilation. This is most likely because higher confining mechanical pressure at deeper levels is unfavourable for tensile failure and associated permeability enhancement. The results of this scenario nicely explain the formation of the Century deposit at the intersection of the TRF with the Little Archie Fault.

In both scenarios described above, fluid mixing at the Pmh4 level potentially involves fluids from different levels of the crust (upflow along deep faults, downflow through the cover unit, and lateral flow along the Pmh4 horizon). It is clear that tensile failure at fault intersections at the Pmh4 level is not due to the relatively lower mechanical strength of rocks. This is demonstrated by the observation that a weaker layer just a few hundred metres below the upper ends of TRF or RL does not show any tensile failure. It is actually the fluid pore pressure build-up at the level of the upper-ends of the blind TRF or RL (buried right below the Widdallion) in combination with the presence of cross faults that played a critical role.

Major points from additional modelling analyses

Additional model scenarios confirmed the significance of the Widdallion Sandstone Member as a strong and relatively-low permeability unit. In a model where the permeability of the Widdallion is increased to values near the permeability of the cover unit, there is no occurrence of tensile failure, permeability enhancement, dilation and fluid focusing/mixing at the Pmh4 level near its contact with the Widdallion unit. Fluid is discharged along faults and through the Widdallion unit to the surface.

To understand the effect of changes in the dips of the TRF and RL, we have constructed the 'H-front' models. The results of the H-front models are consistent with those from the Y-front models (Figs. 2 and 3). However, the development of tensile failure, permeability enhancement and dilation at the Pmh4 level is less extensive in the H-front models than in the Y-front models. This suggests that a Y-front architecture was more favourable for mineralisation in the district, as is also supported by analyses of potential field data.

We have also tested the effects of the D2 event with east-west shortening. The results are generally consistent with the results of the D1 models. It seems that under east-west shortening (D2), however, tensile failure and permeability creation are less extensive at the Pmh4 level than in the equivalent D1 case. This indicates that the D1 compressional direction was more favourable for mineralisation than the D2 compressional direction.

Discussion and conclusions

The concept of tensile failure at the Century deposit requires explanation, given the very fine grained laminated appearance of the mineralisation. Broadbent et al. (1998) observed that zinciferous siderite

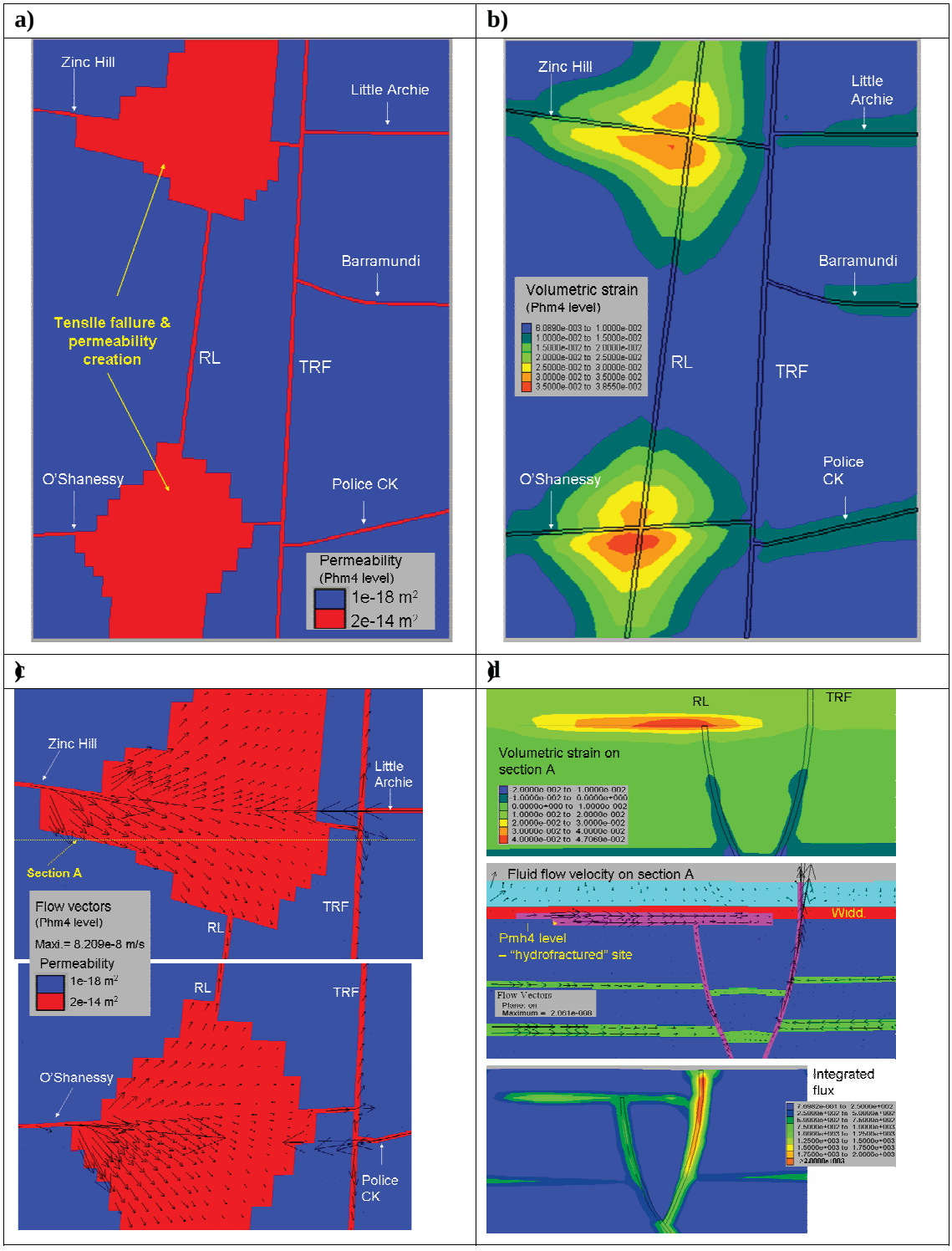

Figure 2. Results of a Scenario-1 Y-front model with buried RL and exposed TRF. a), b) and c) Permeability development, volumetric strain (dilation) distribution and fluid flow patterns at the Pmh4 level, respectively (note tensile failure, permeability enhancement, higher dilation and fluid flow at the intersections of RL with the Zinc Hills and O'Shanessy faults). d) Section plots of dilation, fluid flow vectors and integrated fluid flux.

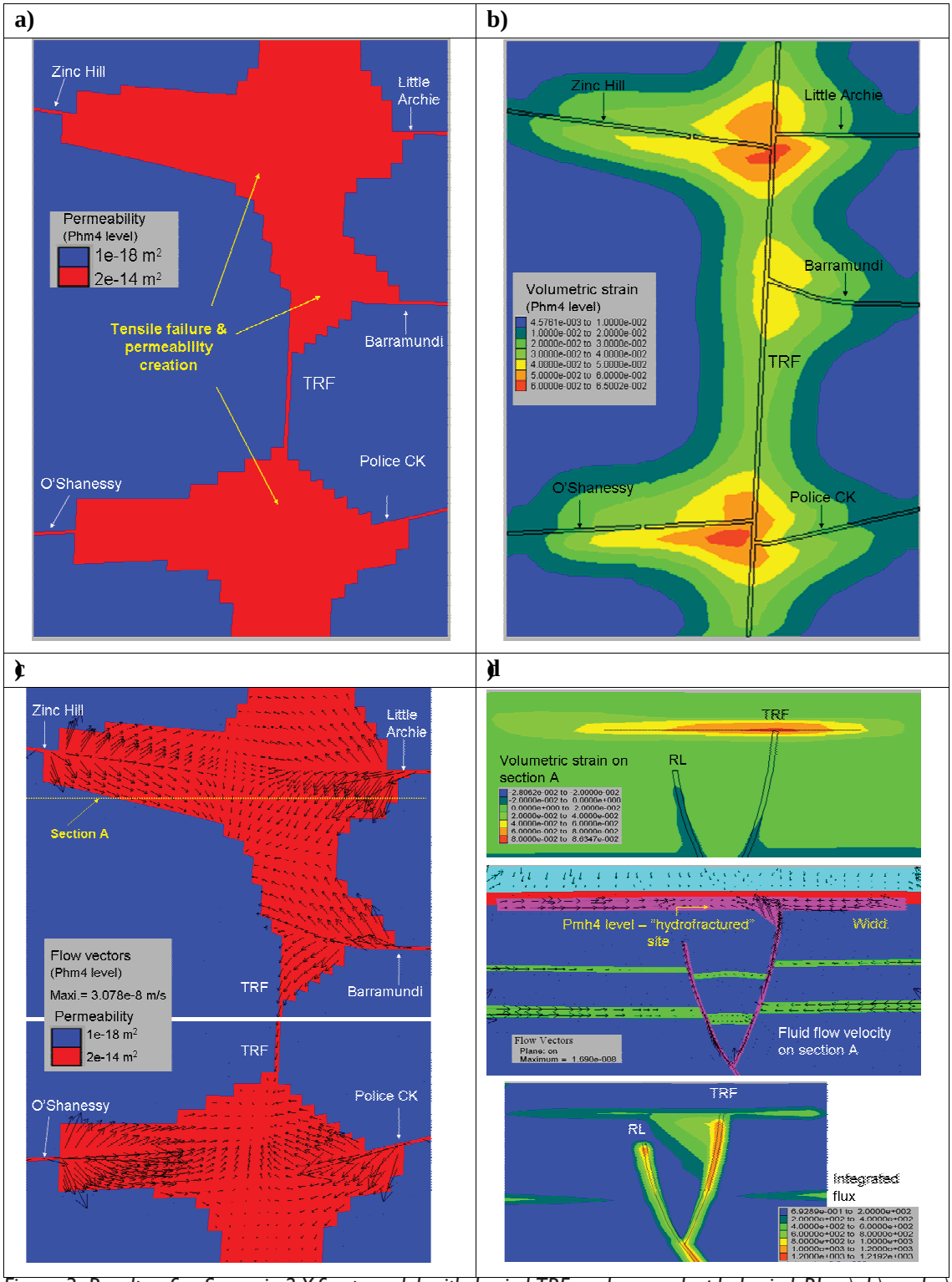

Figure 3. Results of a Scenario-2 Y-front model with buried TRF and more deeply buried RL. a), b) and c) Permeability development, volumetric strain (dilation) and fluid flow patterns at the Pmh4 level, respectively (note tensile failure, permeability enhancement, higher dilation and fluid flow at the intersections of TRF with Police CK, Little Archie and Barramundi faults). d) Section plots of dilation, fluid flow vectors and integrated fluid flux.

overprints compaction fabrics, such as stylolites, but apparently predates the main phase of replacive sulphide mineralisation. There is no evidence of hydrofracturing recorded, although the tensile failure behaviour inferred from our models may have been exposed as a tendency to slightly jack apart bedding parallel surfaces, such as stylolites and bedding planes, to allow the preferential ingress of early zinc-bearing fluids. This helps to satisfy the question why a replacement sulphide body could develop at a site where one impermeable rock is overlain by another. Once this process commenced, chemical reactions and feedbacks may have accentuated the preferability of the mineralised site, and resulted in chemically-induced zinc and lead sulphide precipitation. We do argue, however, that an initial mechanical component to this process was likely required to initiate mineralisation at the top of the thick carbonaceous Pmh4 succession rather than at some point deeper down.

The current modelling results suggest several critical factors for tensile failure, permeability creation, dilation and fluid focusing at the Pmh4 level within the siltstone-shale sequences of the Lawn Hill Formation, and therefore for mineralisation in this horizon:

- A strong and relatively-low permeability Widdallion Sandstone Member. This provides mechanical contrast with the siltstone-shale package below and helps to trap mineralising fluids.
- Blind faults (i.e. faults that do not extend to the surface) are necessary for creating the excess pore fluid pressures that are required for tensile failure. In the cases where the TRF or RL are buried immediately below the Widdallion unit, extensive tensile failure, dilation and fluid focusing/mixing occurred at the Pmh4 level immediately above the upper ends of the blind faults, with clear localisation at the intersections of the TRF or RL with cross faults. This is in contrast to the exposed TRF and RL scenarios where no tensile failure takes place and fluids escape along faults. A blind TRF and/or RL apparently creates a system that is favourable for fluid pore pressure build-up near the upper end of the fault, and hence for tensile failure at the top of the fault. Tensile failure and dilatant sites predicted by the numerical models at the Pmh4 level and inferred to represent mineralised laminae within the shale at Century (Broadbent et al. 1998).
- The burial depth of these faults is also important. Models show that tensile failure does not occur when the RL is buried more deeply. The current results show that ~3 km burial depth is ideal for tensile failure and permeability creation in the shale-siltstone package at the Pmh4 level, which are important for mineralisation in such low permeability rocks.

There are also several important points in the discussion of mineralisation at Century:

- Currently-available geophysical and structural data are insufficient to determine whether the TRF and RL form a Y-front or H-front architecture. Model results suggest that the H-front architecture is less favourable for mineralisation than the Y-front case.
- For the Century district, D1 and D2 shortening both lead to tensile failure and fluid focusing/mixing at the Pmh4 level, when assuming a blind TRF or RL below the Widdallion unit. D1 loading seems to have generated more extensive tensile failure, however, and hence is probably more favourable for mineralisation in the district than D2 loading.
- In a conceptual sense, the TRF and RL (and cross faults) were probably weaker after D1, and easier to propagate towards the surface. This might mean a more open system during D2 and less favourable conditions for mineralisation. In addition, the shortening orientation for the D2 event is more favourable for shear strain localisation (reactivation) along the RL and TRF than that for the D1 event. What we see in the present surface structures of the district is lack of clear, continuous exposure of the TRF (RL does not outcrop). We speculate that the TRF never became fully connected to the surface and the RL is not connected to the surface at all.

The current modelling results reveal only part of the story for the Century mineralisation. The Century ore bodies are hosted within thin shale beds within the top few hundred metres of the siltstone-shale package of the Lawn Hill Formation, but not in direct contact with the Widdallion unit. The models,

however, show tensile failure in the horizon directly beneath the Widdallion unit. Why is this? Mechanically, the horizon in direct contact with the Widdallion unit is the most favourable level for tensile failure. In reality, geochemical controls would have influenced the exact location of mineralisation within the tensile failure horizon. Specifically, the shale beds within this horizon might have been chemically more favourable than the silt beds for mineralisation. A combination of tensile failure and chemically favourable host rocks may have been critical for mineralisation. Geochemical modelling is beyond the scope of the current work, but it is likely that a combination of mechanical and geochemical controls influenced the location of mineralisation at Century.

Acknowledgements

Yanhua Zhang, Paul A Roberts and Barry Murphy would like to thank Zinifex Ltd for funding this work through the *pmd*CRC* G14 project. Heather Sheldon and Guillaume Duclaux are thanked for their reviews and very helpful suggestions and comments.

References

Betts, P.G. & Lister, G.S., 2002. Geodynamically indicated targeting strategy for shale-hosted massive sulphide Pb-Zn-Ag mineralisation in the western Fold belt, Mt Isa terrane: Australian Journal of Earth Sciences, 49, 985-1010.

Broadbent, G.C., Myers, R.E. and Wright, J.V., 1998, Geology and Origin of Shale-Hosted Zn-Pb-Ag Mineralization at the Century Deposit, NorthWest Queensland, Australia. Economic Geology, 93, 1264-1294.

Drummond, B.J., Goleby, B.R., Owen, A.J., Yeates, A.N., Swager, C., Zhang, Y.& Jackson, J.K., 2000. Seismic reflection imaging of mineral systems: three case histories. Geophysics, 65, 6, 1852-1861.

Feltrin, L., 2006. Probabilistic and deterministic models of Pb-Zn mineralisation and post-mineralisation megabreccia, in the Lawn Hill Region, Australia. James Cook University, PhD Thesis.

Feltrin, L., McLellan, J.G. & Oliver, N.H.S., 2007. Modelling the giant, Zn-Pn-Ag Century deposit, Queensland, Australia. Computers & Geosciences, doi:10.1016/j.cageo.2007.09.002.

Itasca Consulting Group, 2005. FLAC3D: Fast Lagrangian Analysis of Continua in 3 dimensions. Itasca, Minneapolis.

Large, R.R., Bull, S.W., Yang, J., Cooke, D.R., Garven, G., McGoldrick, P.J. & Selley, D., 2002. Controls on the formation of giant stratiform sediment-hosted Zn-Pb-Ag deposits: with particular reference to the north Australian Proterozoic. In: Cooke, D. & Pongratz, J., eds, Characteristics, genesis and exploration: CODES Special Publication, 4, 107-149.

Ord, A., Hobbs, B.E., Zhang, Y., Broadbent, G.C., Brown, M., Willetts, G., Sorjonen-Ward, P., Walshe, J.L. & Zhao, C., 2002. Geodynamic modeling of the Century deposit, Mt Isa Province, Queensland. Australian Journal of Earth Sciences, 49, 1011-1039.

Polito, P.A., Kyser, T.K., Golding, S.D. & Southgate, P.N., 2006. Zinc deposits and related mineralization of the Burketown Mineral Field including the world-class Century Deposit, Northern Australia: fluid inclusion and stale isotope evidence for basin fluid sources. Economic Geology, 101, 1251-1273.

Williams, P.J., 1998, An introduction to the metallogeny of the McArthur River-Mount Isa-Cloncurry minerals province. Economic Geology, 93, 1120-1131.

Zhang, Y., Sorjonen-Ward, P., Ord, A. & Southgate, P., 2006. Fluid flow during deformation associated with structural closure of the Isa Superbasin after 1575 Ma in the central and northern Lawn Hill Platform, Northern Australia. Economic Geology, 101, 1293-1312.